Supplementary information

1. Yeast strains and plasmids

1.1 General methods

PCR and subcloning were performed as described elsewhere [1]. Yeast manipulations were performed as described elsewhere [1,2]. Unless otherwise noted, cells were grown in synthetic dextrose complete (SDC) media consisting of Brent Supplemental Media (MP Biomedicals, Solon, OH), yeast nitrogen base without amino acids and ammonium sulfate (BD, Franklin Lakes, NJ), and dextrose (Sigma-Aldrich, St Louis, MO).

1.2 Strains

We list strains used in this study in Supplementary Information Table S1. We used ACL379 as a parent strain, which is derived from YAS245-5C (*can1*::HO-CAN1 *ho*::HO-ADE2 *ura3 ade2 leu2 trp1 his3*), itself a W303 derivative [3].

Construction of TCY3057 is detailed elsewhere [4]. We constructed a *fus3-as2* derivative of this strain, RY2013 in two steps. First, we replaced the *FUS3* gene with a natMX4 cassette [5] by PCR-mediated one-step gene deletion [6], and confirmed deletion both by colony PCR and by altered halos in halo assays [2]. We then digested pES1002 (pRS406-fus3-as2) at a unique MfeI site and then integrated linear DNA into the *FUS3* promoter [2] and selected for colonies that grew on uracil-deficient media. We confirmed integration by identifying cells that displayed 1) pheromone-induced growth arrest and characteristic formation of mating projections ("shmooing") when grown in medium with 100 nM pheromone, and 2) lack of growth arrest and shmooing when grown in medium with 100 nM pheromone and 10 μM 1-NM-PP1. We constructed the Δ*SST2* derivative of this strain, RY2024, by replacing the *SST2* gene with a hphMX4 deletion cassette [5] by PCR-mediated gene deletion.

We constructed the RY1130b in the following way. We first replaced the *DIG1* gene with a kanMX6 cassette [7] and the *STE12* gene with TRP1[7] by PCR-mediated gene deletion. We then linearized pRY1001 (pRS405 P_{STE12}-CFP-Ste12) by digestion with BsiWI, integrated it into the *STE12* promoter, and selected for colonies that grew on leucine-deficient media. We scanned many colonies by fluorescence microscopy and found that the majority of colonies had nuclear CFP fluorescence intensities barely above background, but did express CFP-Ste12, as determined by Western blots using polyclonal rabbit antibodies raised against Ste12 (a generous gift from Ira Herskowitz, UCSF) and monoclonal anti-GFP antibodies (JL-8, Clontech). We picked one of these transformants with low nuclear CFP fluorescence (RY2026) and assumed it contains a single integrated copy of pRY1001. We found two other colonies with apparent integer multiple higher levels of average nuclear CFP intensity, RY2027 and RY2005, which we interpreted as multiple tandem integrations [8] of pRY1001 (two and three copies, respectively). By quantitative Western blots, we measured apparent integer multiple increases in steady-state CFP-Ste12 protein abundance levels in RY2026, RY2027, and RY2005 (Supplemental Materials Fig. 2a), which is also consistent with 1, 2, and 3 integrations of pRY1001, respectively. To create our base FRET strain RY1130b, we first linearized pRY1004 (pRS406 P_{DIG1}-Dig1-YFP) by digestion with BstEII, integrated it into RY2005 in the *DIG1* promoter, and selected for colonies that grew on both leucine- and uracil-deficient media to create RY1130. We confirmed integration of pRY1004 by confirming nuclear YFP fluorescence, and picked a transformant with an average nuclear YFP fluorescence above background that was most common and assumed that this was a single integrant. We then made this strain (RY1130) auxotrophic for uracil by transforming cells with a short PCR product containing 40 bp

homology to both the 5' and 3' ends of the URA3 gene and selecting for colonies that grew on media containing 5-fluoro-orotic-acid (5-FOA, Sigma-Aldrich). We confirmed URA3 deletion by colony PCR and by uracil-dependent growth. RY1130 and RY1130b were indistinguishable using all assays in this work (loss of FRET, MAP kinase phosphorylation, growth arrest, transcriptional output; data not shown).

We also constructed RY2025, a "dark" acceptor version of RY1130 with the YFP in Dig1-YFP containing a Q70N mutation ("YFPdark"[9]; see below), for estimation of FRET efficiency. First, we created RY2005 by plating RY1130 on 5-FOA plates and selecting for colonies that lost the integrated pRS406 P_{DIG1}-Dig1-YFP. We confirmed loss of Dig1YFP by Western blots, using polyclonal rabbit anti-Dig1 antibodies made and characterized by David Pincus and Orna Resnekov (manuscript in preparation). We linearized pRY1004d by digestion at a unique BstEII site and transformed it into RY2005 to make RY2025. We confirmed single integration by comparing Dig1-YFP and Dig1-YFPdark protein abundances in RY1130b and RY2025, respectively, by quantitative Western blots, and then confirmed lack of nuclear YFP fluorescence in RY2025 by fluorescence microscopy. We likewise confirmed identical levels of CFP-Ste12 in RY1130b and RY2025 by quantitative Western blots.

We constructed RY1133b by replacing the endogenous *KSS1* gene in RY1130b with the *kss1-as2* allele in pES1004 (pRS406 kss1-as2-trunc) by two-step integration-excision gene replacement [2]. We similarly constructed RY1134b by replacing the endogenous *FUS3* gene in RY1130b with the *fus3-as2* allele from pES1002 (pRS406 fus3-as2), and RY1137b by similarly replacing *FUS3* in RY1133b with *fus3-as2*. We linearized pES1004 plasmid DNA by digesting at a unique BsiWI to integrate in the 5' end of the *KSS1* gene, upstream of the E94A mutation site; for pES1002, we digested with MfeI to integrate into the *FUS3* promoter region (1000 bp region upstream of the start codon). We confirmed gene replacement by altered DdeI restriction digestion patterns of colony PCR products. We made RY1135b by replacing the *KSS1* gene in RY1134b with an hphMX4 cassette using PCR-mediated gene replacement.

We made versions of RY1130b, RY1135b, and RY1137b with P_{PRM1}-YFP transcriptional reporters (RY1130bPY, RY1135bPY, and RY1137bPY, respectively) by replacing the *PRM1* open reading frame in each with a YFP-His3MX6 cassette from pYFP-His3MX6 [3] by PCR-mediated gene replacement.

We made strains RY700, RY701, RY702, RY2052b, RY2053, and RY2055 from the W303 derivative ACL387 [10]. To make RY700, we deleted *FUS3* in ACL387 by PCR-mediated gene replacement with a *TRP1* cassette [7]. To make RY701, we deleted *KSS1* in ACL387 by PCR-mediated gene replacement with a *TRP1* cassette [7]. To make RY702, we deleted *KSS1* in RY700 by PCR-mediated gene replacement with a kanMX6 cassette [7]. RY2052b was made by replacing *FUS3* in ACL387 with the *fus3-as2* allele by two-step integration-excision gene replacement [2] using plasmid pES1002. We made RY2053 by deleting *KSS1* in RY2052b by PCR-mediated gene replacement with a kanMX6 cassette. RY2055 was made by replacing *KSS1* with the *kss1-as2* allele in RY700 by two-step integration-excision gene replacement [2] using plasmid pES1004.

We made RY2073 by integrating pGP1001 into TCY3154 [10]. To do this, we linearized the plasmid at a unique AvrII restriction site in between the two *LYP1* sequences and transformed yeast with the linearized plasmid. We selected for integrants by plating the cells on uracil-deficient plates containing the toxic lysine analog thialysine, which selected for the presence of the *URA3* cassette and for the

absence of *LYP1* function. We confirmed integration by checking that the thialysine resistant strains expressed mRFP constitutively by microscopy.

We made RY2077 (*sst2-T134A)* in two steps. First, in TC3057, we replaced the nucleotides corresponding to threonine 134 in *SST* with the *Candida albicans URA3* knockout casette [11] by PCR-mediated gene replacement. We confirmed integration by PCR and by increased sensitivity to pheromone in halo assays, indicative of a disruption in Sst2. We then replaced the inserted *URA3* sequence by transforming, into this strain, a double-stranded oligonucleotide consisting of 40 nucleotides upstream of the nucleotides corresponding to threonine 134 in *SST2*, the nucleotides GCA (corresponding to an alanine), and 40 nucleotides downstream of amino acid 134 in *SST2*. We selected for transformants by growth on media containing 5-FOA. We confirmed the *T134A* mutation by direct sequencing.

1.3. Plasmids

We list plasmids used in this study in Supplementary Information Table S2. In order to make pES1002 and pES1004, we performed PCR-mediated mutagenesis to introduce a Q93A mutation into Fus3, previously identified as a sensitizing mutation [12], and an E94A mutation in Kss1, identified by sequence alignment with Fus3, using ACL379 genomic DNA as a template. For pES1002, we included 1000 bases of sequence upstream of the start codon and 401 bases downstream of the stop codon in addition to the gene; for pES1004, we included bases 22-1107 from the KSS1 gene and 401 bases downstream of the stop codon. We also introduced a 5' KpnI restriction site and a 3' NotI restriction site to each PCR product. We then subcloned these into pRS406 vectors cut with KpnI and NotI. We confirmed correct coding region sequences by direct sequencing.

We made pRY1001as follows. First, using ACL379 genomic DNA we amplified the *STE12* gene, including the stop codon. We used a 5' primer that included 40 bases of the 3' end of YFP in pACL7-YFP-A206K [3], an AsiSI restriction site, and a single T to make *STE12* in-frame with YFP, and we used a 3' primer that included 40 bases downstream of the XhoI restriction site in pACL7-YFP-A206K. We cloned this PCR product, by homologous recombination, into pACL7-YFP-A206K linearized by XhoI. We did this by co-transforming ACL379 with linearized pACL7-YFP-A206K and the PCR product, selecting for colonies that grew on uracil-deficient media, and recovering pRY1001 candidate plasmids [1] from transformants identified by colony PCR. We isolated a plasmid containing the *STE12* open reading frame and confirmed the *STE12* sequence by direct sequencing. We then PCR amplified and subcloned 1000 bases of DNA upstream of the *STE12* start codon, and introduced on the 5' and 3' ends KpnI and EcoRI sites, respectively. We subcloned this PCR fragment into KpnI/EcoRI sites of the recovered and sequenced plasmid, digested this with BglI and isolated the large fragment. We then subcloned this fragment, containing P_{STE12}-YFP-STE12-TADH1, into the small BglI fragment from a BglI digest of pRS405 plasmid DNA [13]. Finally, we swapped YFP-A206K with CFP (ECFP from Clontech) by subcloning, into the large fragment from an EcoRI/AsiSI digest of this plasmid, PCR-amplified CFP, flanked by a 5' EcoRI sequence and a 3' AsiSI site, to yield pRY1001.

We made pRY1004 in a similar fashion. We PCR amplified *DIG1*, using a 5' primer consisting of 40 bases upstream of the YFP-A206K start codon in pACL7-YFP-A206K, and an AscI restriction site, and using a 3' primer containing 40 bases of the 5' end of YFP-A206K in pACL7-YFP-A206K. We subcloned, by homologous recombination, this PCR product into pACL7-YFP-A206K that we

linearized by digestion with EcoRI. We isolated *DIG1*-containing plasmids in a manner similar to pRY1001, and confirmed the proper sequence of *DIG1* by direct sequencing. We similarly subcloned the *DIG1* promoter (1000 base region upstream of the *DIG1* start codon) into the KpnI/EcoRI sites of this plasmid, and then subcloned the large fragment of this plasmid digested with BglI into the small BglI fragment of pRS406[13] to yield pRY1004. We then made pRY1004d (pRS406 P_{DIG1}-Dig1-YFPdark), which is pRY1004 containing a version of YFP with a Q70N mutation [9], by PCR-based mutagenesis.

To make plasmid PGP1001 we first replaced YFP open reading frame in pRS406-pACT1-YFP [10] with the mRFP [14] open reading. We synthesized a modified open reading frame coding the same mRFP polypeptide, codon optimized for *S. cerevisiae*. We accepted delivery of this synthesized yeast-optimized mRFP coding DNA from Blue Heron Inc. At a unique Aat II site in the resulting plasmid, we inserted a 222 bp segment of synthetic DNA containing the following elements: 100 bp of the sequence that follows the stop codon of the *LYP1* open reading frame, a series of restriction sites and 100 bp of the sequence that precedes the start codon of the *LYP1* open reading frame. In pGP1001, the coding strand of the LYP1 sequences was the same as that of the ACT1 sequence.

2. Single cell microscopy methods

2.1. Image acquisition and data analysis

Procedures were built on those in prior work [3,4,10]. Briefly, we collected images using a Nikon TE300 inverted fluorescence microscope with a Nikon PlanApo oil-immersion 60X objective (NA=1.4). We controlled bright field and fluorescent lamp shutters (Uniblitz, Rochester, NY), and a six position linear cube changer (Conix Research, Springfield, OR) with Metamorph version 6.2 (Molecular Devices, Sunnyvale, CA), and auto-focused using a custom routine (derived from [4]) written in Visual Basic (Microsoft, Redmond, Washington).

To prepare cells for measurement, we first sonicated 150 μl of exponentially growing cells (OD_{600nm} = 0.4-0.8) briefly in 1.5 ml Eppendorf tubes in a Misonix Sonicator 3000 water bath Misonix Inc., Farmingdale, NY) for 30 seconds at output setting 1.0 to separate clumped cells. We then deposited cells into one well of a black-walled, glass-bottomed 96 well sample plate (Arctic White LLC, Bethelehem, PA) that we had pre-treated for at least 15 minutes with 100 μl of 0.1 mg/ml concanavalin V (Sigma) in water. After 10 minutes, we washed immobilized cells three times with 100 μl of media. (We scaled up appropriately for experiments requiring data collection from multiple wells).

We extracted parameters of interest from images using Cell-ID 1.0[15] and analyzed them using Physics Analysis Workstation (PAW)[16] and custom scripts. Image files, Cell-ID input scripts and PAW analysis scripts are available upon request.

For *fus3-as2* Δ*sst2* cells (RY2024), we used the following procedure to reduce the accumulation of hypersensitive Δ*sst2* cells that accrue loss-of- function mutations in system components that allow cells overcome Fus3-mediated cell cycle arrest. We prepared the cells as above with the following modifications. First, we included 10 μM 1-NM-PP1 in media while growing cells up to a suitable culture density range. We then pelleted the cells gently by centrifugation, washed in synthetic defined growth media without inhibitor, diluted the cells to 0.05 OD600nm, and grew the cells for another 3-4 doublings. We then continued with the experiments as outlined below.

2.2. Fluidic control

We constructed a custom fluidic injection and evacuation device [17] to automatically apply liquids to and remove liquids from the bottom of a well in a 96-well glass bottom sample plate. The system consists of a head that holds up to eight 0.1 mm diameter lengths of tubing with ends manually positioned at desired heights above the well bottom. Each of the lines passes through a valve and either terminates in a vial containing pressurized liquid to be applied to the cells, or in a vacuum trap. Media vials are pressurized with 15 psi of compressed air and can inject approximately 100 μl/sec of 1X BSM-2% glucose media containing pheromone and/or inhibitor. The bulk of the head sits in a well adjacent to the well under observation and minimally interferes with the overhead bright-field light source. The tubing is situated along the edge of the observation well and is non-reflective; it does not measurably contribute to background in any of the CFP, YFP, RFP, or FRET fluorescence measurements (data not shown). Valves are controlled using Metamorph. Further details are available upon request.

2.3. YFP-Ste5 translocation quantification

Ste5 protein is present at very low numbers. There are ~500 molecules per cell on average, and due to significant YFP fluorophore maturation times, when Ste5 is tagged with YFP only ~350 of 500 YFP-Ste5 are fluorescent in exponentially growing cells [4]. In these cells, the fluorescence signal from YFP-Ste5 molecules is barely above background autofluorescence. To increase the signal-to-background ratio, we constructed a strain that expressed two copies of chromosomally integrated *YFP-STE5* expressed from native promoter sequences. Doubling the gene dosage increased the signal-to-noise ratio while only modestly perturbing levels of Ste5 and system activity, as reflected by the amount of reporter gene output (about 1.5 times wild-type cells, data not shown).

For each of the time courses presented, we measured at least three observation fields, each containing 20-150 cells, for each stimulus condition. For each time point, we auto-focused, took a 0.25 sec YFP exposure, a focused bright field image (to allow later confirmation of the focus for the timepoint's fluorescence image), and a defocused bright field image (for cell identification and boundary determination). We identified the cell boundaries in the bright field image using Cell-ID, and defined a ring of pixels 1 pixel outside (i.e. away from the cell center) of this boundary as the "membrane region." We manually confirmed that the automatically determined membrane region overlaps with observed fluorescent pixels in images of cells with YFP targeted to the cell membrane (data not shown). We defined the level of membrane recruitment *M(t)* as the fractional change in total membrane region fluorescence F_M from pre-stimulated cells (t=0).

$$(2.3.1)\quad M(t) = \frac{\left(F_M(t) - F_M(t_0)\right)}{F_M(t_0)}$$

where F_M is defined, per cell, as the total fluorescence of the membrane region minus the calculated area of the membrane region times the average extracellular per-pixel-background in the image. We observed that total cellular fluorescence dropped off rapidly for the first 15 exposures and then decayed with smaller percentage per exposure afterward. We attribute this two-phase loss of fluorescence to efficient and rapid photobleaching of auto-fluorescent components in addition to YFP photobleaching for initial exposures, and photobleaching of predominately YFP for later exposures. Thus, for all time courses we collected 15 time points prior to cell stimulation and measurement. We then took two baseline images, stimulated cells with appropriate media conditions, and then took images at indicated times. In order to

correct for photobleaching, we performed a double-exponential fit to the median data collected from timecourses in which we did not perform any stimulation (Fig. S3e, gray line). We then subtracted this fit from all of the other timecourses (pheromone, pheromone + inhibitor, inhibitor only, or no treatment; see Fig. S3e) to produce data corrected for photobleaching as presented in the main text figures. We performed an independent correction based on a "no treatment" timecourse for each experiment in order to minimize effects of variation in lamp strength (and thus variations in photobleaching) between experiments.

The total number of fluorescent molecules at the membrane in the focal plane is quite low. We roughly estimated this number in the following manner. We first estimated the fraction of the cell surface within focal plane, which we estimated for our equipment to be ~2 μm thick [4]. We considered the average yeast cell to be spherical with a 5 μm diameter and a total area of about 80 μm^2. If the focal plane is positioned to perfectly bisect the cell, the area of this sphere in the 2 μm thick focal plane is ~60 μm^2. ~75% of the total area. If we assumed that 1) upon pheromone stimulation, YFP-Ste5 molecules translocated randomly and isotropically, thus evenly distributing themselves over the interior of the whole cell surface, and 2) after translocation, they are essentially motionless during the course of an exposure (250 ms), then 75% of the total number of YFP-Ste5 molecules are in the focal plane, or about 750 out of 1000 YFP-Ste5 molecules per cell in the 2x *YFP-STE5* strains used in this work [4]. Of these, due to YFP fluorophore maturation times ($t_{1/2}$=39 ±7 min for the YFP used in this work in yeast), only 70% of these are fluorescent at any given time in exponentially growing cells [4], reducing the number of fluorescent YFP-Ste5 molecules in the focal plane to ~525.

2.4. FRET quantification

We measured time courses for at least three observation fields, each containing 20-150 cells, for every stimulus and perturbation condition. For each time point, we auto-focused, took a focused bright field image (to allow later confirmation of the focus for the timepoint's fluorescence image), a defocused bright field image (for cell identification and boundary determination), a 0.2 sec CFP excitation image with the emission image split into CFP and YFP emission channels (Dual View image splitter, Optical Insights), and a 0.5 sec YFP excitation/YFP emission image. We used the following filters and dichroic mirrors (Chroma): CFP excitation, 435/40X; CFP emission, 480/30M; YFP emission, 525/30X, 535/20M; beam splitter dichroic, DX505.

For all fluorescence images, to limit fluorophore photobleaching, we used an ND4 neutral density filter. We measured a 1.4% loss of nuclear CFP signal and 0.6% loss of nuclear YFP signal for each subsequent time point. However, as with Ste5 translocation, we observed that some auto-fluorescent components were rapidly photobleached after five initial sets of exposures; during this phase, the calculated FRET exponentially decreases; after the five exposure "pre-bleach", calculated FRET values remain stable for unstimulated cells. Thus, we performed five sets of exposures for each field before data collection. Then, we took two baseline image set followed by an additional set every 30 seconds, with stimulations automatically applied at indicated times.

We define a FRET statistic, F, based on N_{FRET} (Xia and Liu, 2001), with FRET signal (that is, YFP emission resulting from CFP excitation) normalized by both acceptor and donor concentrations. We define F *as*

(2.4.1) $$F = \frac{CY}{\sqrt{CC \times YY}}$$

We define CY, the corrected signal resulting from illumination at the CFP excitation wavelength and measuring in the YFP emission channel, as

(2.4.2) $CY = CY_{obs} - B_{CY} - A_{CC \rightarrow CY}(CC_{obs} - B_{CC})$

and CC, the corrected signal measuring in the CFP emission channel, is defined as

(2.4.3) $CC = CC_{obs} - B_{CC} - A_{CY \rightarrow CC}(CY_{obs} - B_{CY})$

There is significant CFP emission crosstalk into the YFP emission channel due to its broad emission spectrum ("spectral bleedthrough"); for example, an image of a sample containing purified CFP protein, using CFP excitation wavelengths, will show up as a measurable signal in the YFP emission channel. We measured the emission crosstalk parameter $A_{CC \rightarrow CY}$, the ratio of YFP emission channel signal to CFP emission channel signal for pure CFP emission, for our optical setup using his-tagged CFP that we recombinantly expressed and purified, to be 0.99 (data not shown). $A_{CY \rightarrow CC}$ is negligible (see image segment labeled "YC" in Supplemental Fig. S6b, simplifying (2.4.3) to

(2.4.3b) $CC = CC_{obs} - B_{CC}$

We similarly define corrected YFP nuclear fluorescence using YFP excitation as

(2.4.4) $YY = YY_{obs} - B_{YY}$

Equations (2.4.2)-(2.4.4) contain terms B_{CC}, B_{CY}, and B_{YY} to correct for background cellular fluorescence in each emission channel. We calculate these quantities by taking the average fluorescence of pixels in a 1 pixel-wide ring with a radius of 6 pixels centered on the calculated center of the nucleus. This is a reliable per-cell predictor of nuclear background signal; we found that, in wild-type cells with unlabeled Dig1 and unlabeled Ste12, CFP or YFP are relatively flat throughout the cell interior in the CY, CC, and YY channels (data not shown). F is unitless and compensates for differential photobleaching of CFP and YFP by all exposures for a given time point, in the sense that F remains flat for unstimulated cells.

For examples of raw values of these values used in the calculation of F for pheromone-stimulated and unstimulated cells, see Supplemental Tables S4 and S5, respectively. Aiming for as unbiased an analysis as possible, we rejected cells based on parameters that are only indirectly related to the FRET calculation, such as cell area, or based on values of directly involved parameters out of mathematical necessity, such as ensuring positive values in the denominator of Eq. 2.4.1. In the figures presented in the main text, we displayed median values, which are less resistant to outliers; however, as shown in Tables S4 and S5, the mean and median values show the same trends, and choosing median instead of mean values does not affect the conclusions presented in this work.

For analysis of the Gpa1-Ste18 FRET strain (RY2062b), we performed the procedure outlined above, except that instead of using nuclear fluorescence values for the various wavelength channels, we used fluorescence values from membrane-associated pixels using Cell-ID [4] as described above in the section discussing YFP-Ste5 membrane recruitment.

2.5. P_{PRM1}-(FP) quantification

We performed quantification of fluorescence protein-based transcriptional reporters as previously described [3,10,15], except that did not perform minor corrections for light from out-of-focus regions of the cell. This modification does not effect the conclusions of our work as presented.

3. MAPK phosphorylation quantification

3.1. Protein sample preparation

For each time point, we mixed 1.0 ml of exponentially growing cells (OD_{600nm} = 0.4 - 0.8) with 82.5 µl of 10M NaOH and 10 µl of 100% 2-mercaptoethanol (premixed immediately before the experiment). We incubated samples at room temperature for 5 minutes, added 150 µl of 100% trichloroacetic acid, electrophoresis grade (Sigma-Aldrich, St. Louis, MO), mixed samples well and incubated them on ice for 10 minutes. We then centrifuged samples at >10,000 g for 2 minutes, aspirated the supernatant, incubated the pellet with ice cold acetone for 5 minutes on ice, re-centrifuged to pellet the cells, aspirated the acetone, and allowed the pellet to air dry. We prepared samples for electorphoresis by resuspending pellets in 50 µl of SDS-PAGE loading buffer (10 mM Tris pH 8.8, 0.002% bromophenol blue, 100 mM dithiothreitol, 2% SDS, 50% glycerol) per sample, sonicating to completely disperse cell pellets using a Misonix Sonicator 3000 water bath for 60 seconds at output setting 10.0, and boiling for 5 minutes. Samples were quickly spun at >10,000xg in a microcentrifuge to clear cellular debris before electrophoresis.

3.2. Quantitative immunoblotting- electrophoresis, Western transfer, and quantification

We electrophoresed protein samples using 4-15% Tris-HCl/glycine polyacrylamide gels (Bio-Rad, Hercules, CA), then transferred proteins onto 0.2 µm Immobilon-P(SQ) PVDF membrane (Millipore, Billerica, MA) for 45 minutes at 225 mA using a Mini Protean Western transfer system (Bio-Rad). We then blocked membranes for at least 1 hour at room temperature in Tris-buffered saline (TBS, 10 mM Tris pH 7.4, 150 mM NaCl) plus $1/10^{th}$ volume of Western Blocking Reagent (WBR) (Roche, Alameda, CA). We first quantified both phosphorylated and total Fus3 and Kss1 by simultaneously probing with rabbit anti-phosphoP44/P42 #9101L at 1:1000 dilution (Cell Signaling Technology, Danvers, MA), goat anti-Fus3 #sc6773 at 1:500 dilution (Santa Cruz Biotechnology, Santa Cruz, CA), and goat anti-Kss1 #sc6775 at 1:200 dilution (Santa Cruz Biotechnology) overnight at 4 °C, diluted 1:1000, 1:500, and 1:200 respectively in primary antibody binding buffer (TBS, $1/10^{th}$ volume WBR, and 0.05% Tween). We then washed blots in TBS and probed for 1 hour at room temperature with 800 nm donkey anti-rabbit #611-731-127 (Rockland Inc., Gilbertsville, PA) and 680 nm donkey anti-goat A21084, fluorophore-conjugated secondary antibodies (Invitrogen, Carlsbad, CA) , diluted 1:10,000 in secondary antibody binding buffer (TBS, $1/20^{th}$ volume WBR, 0.025% Tween and 0.01% SDS). Blots were washed in TBS then scanned on a LiCor infrared imaging system (Li-Cor Biosciences, Lincoln, NE). We then prepared blots for quantifying PGK as a loading control using mouse monoclonal anti-PGK1 A-6457 (Invitrogen), either by probing identically prepared transfers or by stripping previously probed blots by shaking in stripping buffer (62.5 mM Tris pH 6.8, 2% SDS, and 100 mM 2-mercaptoethanol) at 50 °C for 30 minutes, washing extensively with TBS, and re-blocking. Before re-probing, stripped blots were scanned to ensure that >95% of previously observed signal was removed at regions around PGK (~50 kDa apparent mobility). We then probed with mouse anti-PGK for 1 hour at room temperature,

followed by 800 nm donkey anti-mouse secondary antibody #610-731-124 at 1:10,000 dilution (Rockland), washed, and scanned as described above.

We quantified band intensities using Odyssey v1.2 (Li-Cor Biosciences) using median top/bottom background correction.

4. mRNA quantification by ribonuclease protection assay

We treated 10 ml of exponentially growing cells with 100 nM pheromone, and then separated cells from media by vacuum filtration onto 0.45 μm filter discs (Millipore). We put the discs with cells into 1.5 ml Eppendorf tubes and flash-froze at the indicated times after stimulation with pheromone by immersing open-capped tubes in liquid nitrogen. For total RNA extraction, we thawed samples on ice and used RiboPure Yeast kit (Ambion, Austin, TX). We broke cells open using a Mini-bead-beater-8 (Biospec Products, USA) using 400 ul of 0.45 μm glass beads (Sigma) by agitating for 1 minute. We generated radioactive probes for *ACT1* (loading control) and *FUS1* using αP^{32} dCTP (GE Healthcare) and performed ribonuclease protection assays using a RPA III kit (Ambion, Austin, TX). We electrophoresed samples on a 5% TBE/polyacrylamide gel, dried the gel for 1 hour at 65 °C, and exposed the gel to a phosphorimaging plate (GE Healthcare) for 12 hours at room temperature. We scanned the plate on a Storm scanner (GE Healthcare) and quantified bands using ImageJ [18].

5. RY1130b (FRET strain) characterization

The strain with the best loss of FRET signal responded normally to pheromone in terms of growth arrest (Fig. S5a and Supplementary Information 5). The sensitivity (EC50) of the response using transcriptional reporter gene expression assays was similar to the response in reference strains with unlabeled Dig1 and Ste12. The relative magnitude of the response was about three times higher at all doses (Fig. S5b). We found that this reporter strain and derivatives (RY1130 and related strains) expressed levels of Ste12 protein consistent with multiple (three) integrated copies of *CFP-STE12* (Fig. S5c). Levels of nuclear CFP fluorescence remained stable over many rounds of cell division and many months of laboratory manipulation, indicating that the cells stably maintained multiple *CFP-STE12* copies (data not shown).

Pheromone-induced loss of FRET is dependent both on the presence of Ste5 (Fig. S7c) and on MAP kinase activity (Fig. S7d). Based on median nuclear CFP fluorescence values (see Supplementary Table S3) from RY1100 (Δ*DIG1* Δ*STE12*), RY1130b (base FRET strain), and RY2025 (FRET strain with Dig1-YFP replaced by Dig1-YFPdark at equivalent protein levels, see Supplementary Fig. S7c), we estimate the average FRET efficiency,

$$(5.1)\quad E = 1 - \frac{CC_{DA}}{CC_{D}}$$

where CC_{DA} is the nuclear fluorescence of the donor in the presence of an acceptor (RY1130b) and CC_{A} is the nuclear fluorescence of the donor without an acceptor (RY2025), corrected for autofluorescence values (RY1100), in un-stimulated cells to be approximately 8% (data not shown). This is consistent with FRET efficiency estimates based on acceptor photobleaching studies (data not shown).

6. Measurement of dose-responses using high throughput flow cytometry

6.1 Pheromone induction in multiwell plates

We performed flow cytometry experiments in 1 ml-capacity 96-well polypropylene plates. We first sonicated exponentially growing cells in individual 1.5 ml microcentrifuge tubes, as described above. We then added 10 μl of sonicated cell culture to 200 μl of media with 0.15X Dulbecco's phosphate-buffered saline and 20 μg/ml casein (Sigma) containing 5 μM 1-NMPP1 (to inhibit *cdc28-as2*) and the appropriate concentration of pheromone. We incubated plates at 30 ºC in an air-heated shaker rotating at 300 rpm. After 3 h, we added 10 μl of 500 μg/ml cycloheximide. We incubated the plate for at least 5 h to allow for complete maturation of the fluorescent protein fluorophores. Within that time period we sonicated the plate. We drilled 3/8" holes in each of the corners to ensure that all the liquid in all wells were completely submerged in the sonicating bath. We then sonicated as described above, except we that sonicated for two minutes at power 8.

6.2 High throughput sampling into the flow cytometer

We transferred the cycloheximide-treated cells to 350-μl capacity 96-well polycarbonate plates. We moved individual wells into the flow cytometer using a custom-built, attached high-throughput sampler (HTS). The HTS was set to high-throughput mode and programmed to mix the well and collect 5 μl in 10 seconds (500-5000 cells), followed by three 200 μl washes.

6.3 Flow cytometric measurements

We used a Becton-Dickinson LSRII flow cytometer equipped with a 100 mW 488 nm laser and a 150 mW 532 nm laser. All filters and dichroic mirrors were from Chroma.We used a threshold value of forward scatter (FSC) from the 488 nm laser to trigger data collection. We calibrated threshold values of FSC to detect the smallest cells in an exponentially growing culture of wild type yeast cells or equivalent. We measured YFP and mRFP fluorescence from the light emitted during the 532 nm excitation, which was channeled, using mirrors, into an octagonal array of 8 photomultiplier tubes (PMTs), labeled A to H. Light entering the array is first split by a 735 nm long-pass dichroic mirror (735LP) and then split again by a 640 nm long-pass dichroic mirror (640LP). The light that goes through the 640LP dichroic is filtered through a 675 nm band-pass filter of 50 nm wavelength width (675/50) before hitting the B PMT. The lower wavelength light that reflect in the 640 LP dichroic is directed towards a 600LP dichroic, the reflected light is split by a 540LP dichroic. The light that goes through the 540LP dichroic is filtered through a 550 nm band-pass of 10 nm width (550/10) before hitting the D PMT.

We took the signal from the B PMT as the fluorescence from mRFP. Cells expressing only YFP or CFP show the same signal in this channel as wild type cells. We took the signal from PMT D as the fluorescence from YFP. Cells expressing only mRFP or CFP show the same signal in this channel as wild type cells.

7. Hill function fits and parameter calculations.

We fit data with Hill functions and calculated EC50 and Hill coefficient values using commercial software, Prism 4 (Graphpad Software Inc., San Diego) and ProFit (QuantumSoft, Uetikon am See,

Switzerland). Using default settings and similar initial values for fitting routines, we calculated essentially the same values described in the text using either program.

8. How negative feedback can improve information transmission

Here we discuss how negative feedback help stabilize output (and thus increase the signal-to-noise ratio) of biological systems , which can have substantial cell-to-cell variation in component number [19]; for example, we have observed significant cell-to-cell variation in protein levels of components in the yeast pheromone response system (Thomson, personal communication and [4]), as well as increase the signal-to-noise by increasing the dynamic range of the output relative to noise in the output.

8.1 Negative feedback makes system output robust to variation in component properties

Negative feedback can stabilize the input-output relationship of a system given substantial variation in component properties. This fact, and its relevance to design of electronic amplifiers, was noted by Harold Black[20]. Savageau [21], in a theoretical study, analyzed how, in a transcription system expresses its own repressor, the system's negative autoregulation decreases the variability of repressor protein output levels. Experimental analyses of synthetic gene regulatory circuits confirmed this concept [22]. In a theoretical study, Barkai and Leibler also proposed that non-transcriptional negative feedback stabilized output of biochemical networks, such as in the two-component signaling system that mediates bacterial chemotaxis [23].

8.2. Negative feedback can bring about dose-response alignment without eliminating output dynamic range

A classic analysis of operational models of multi-step biochemical systems [24] indicated a tradeoff between dose-response alignment of upstream and downstream responses and the dynamic range of the downstream response. A reduced output dynamic range reduces the signal-to-noise ratio in systems where output has a minimum level of noise that does not scale with system output. Specifically, Black and Leff analyzed a series of operational models of pharmacological agonist and related applied agonist dose to the observed effect [24]. We show in Fig. S1 a simple model from their work of a response system with two signaling steps. Each step is a mass-action-based reaction that we describe by a hyperbolic, Michaelis-Menten-form relationship.

$$(8.1)\quad [AR] = \frac{[R_0][A]}{K_1 + [A]}$$

Eq. 8.1 describes the dose-response of the first step, receptor-agonist binding, where [AR] is the concentration of agonist-receptor complex, $[R_0]$ is the concentration of total receptor, [A] is agonist concentration, and K_1 is the dissociation constant for this interaction.

$$(8.2)\quad E \propto [ART] = \frac{[AR]}{K_2 + [AR]}$$

Eq. 8.2 describes the second step, formation of the agonist-receptor-transducer (ART) as a function of AR, and the effect (E), which is proportional to the concentration of ART. K_2 is the dissociation constant of this reaction.

Black and Leff combined Eqs. 8.1 and 8.2 to express [ART] as a function of [A] instead of [AR].

$$(8.3)\quad E \propto [ART] = \frac{[R_0][A]}{K_1K_2 + ([R_0] + K_2)[A]}$$

Dose-response alignment, as we discuss in this work, manifests in this system when the EC50 of the effect E as a function of agonist concentration approaches EC50 of the first step (i.e., K_1). The slopes match because the dose-responses of [AR] and [ART] and hyperbolic (i.e., have the same Hill coefficient).

Black and Leff showed that the concentration of agonist yielding half-maximal effect E is

$$(8.4)\quad EC50 = \frac{[K_1]}{1 + ([R_0]/K_2)}$$

This relationship shows that, as the doses align (EC50 approaches K_1), $[R_0]/K_2 \to 0$.

The magnitude of the maximal effect, E_{max}, is defined by

$$(8.5)\quad E_{\max} = E_{[A]\to\infty} \propto \frac{1}{1 + (K_2/[R_0])}$$

Thus, as dose-responses align and $[R_0]/K_2 \to 0$, $K_2/[R_0] \to \infty$, and $E_{\max} \to 0$.

Dose-response alignment is equivalent to saying that there is a linear transfer function between [AR] and E. However, as defined in Eq. 8.2, the transfer function between [AR] and E is hyperbolic. One way to get a linear response from a hyperbolic transfer function is to only sample a very small part of the transfer function with small values of [AR]. In this range of input, the transfer function is approximately linear, but then the outputs are accordingly restricted to small values.

9. Application of metrics from information theory to quantify how well cell signaling systems transmit information about external conditions

Mutual information from information theory [25] can quantify how well a cellular signaling system can transform inputs, such as a distribution of receptor occupancies in pheromone response, into distinguishable outputs, such as corresponding distributions of output from a transcriptional reporter gene.

In the continuous case, we compute mutual information (in bits) based on the following definition:

$$I(D,R) = \iint \varphi(d,r)\log_2\left(\frac{\varphi(d,r)}{\varphi(d)\varphi(r)}\right) dd\, dr,$$

where $\varphi(d,r)$ is the joint dose-response probability density function, and $\varphi(d) = \int \varphi(d,r)\, dr$ and $\varphi(r) = \int \varphi(d,r)\, dd$ are the marginal density functions for dose and response, respectively. Since our experimental data typically consists of observed responses to applied doses, we use another form of this

double integral that emphasizes the distribution of responses conditional on the application of a given dose d, that is, $\varphi(r \mid d) = \varphi(r,d)/\varphi(d)$:

$$I(D,R) = \int \varphi(d) \left(\int \varphi(r \mid d) \log_2 \left(\frac{\varphi(r \mid d)}{\varphi(r)} \right) dr \right) dd .$$

The mutual information captures how the graded-ness of the response and the noise of the response impact the overall ability of cells to distinguishably respond to different external pheromone concentration. For example, consider two cell types, each with the same graded pheromone-receptor binding response. A cell with low transmission noise but an extremely switch-like downstream response has a reduced ability to respond differently to different doses, because all inputs are restricted to only one of two responses. On the other hand, a cell with a graded downstream response and high transmission noise also has a reduced ability to respond differently to different doses, because transmission noise increases the variation in the responses, making it harder to determine if a given response is associated with a particular input. The diminished ability to respond distinctly to a particular set of input pheromone concentrations would be reflected by lower mutual information scores calculated for both cell types.

Mutual information also quantifies how the actual choice of pheromone concentrations the system is responding to affects the ability of the system to generate distinguishable responses. For example, if we stimulate the system using input concentrations that yield saturated responses (such as stimulating Δ*sst2* cells with pheromone concentrations that are within the dynamic range of receptor occupancy but saturate the downstream response), then the responses are nearly indistinguishable, and provide little information about the external pheromone concentration. In this case, the mutual information would be low.

A special case of mutual information called the channel capacity (Part IV, section 24 in [25]). This represents how much information the system can transmit considering all possible input doses. This metric reflects the fundamental ability of a system to transmit information about external conditions given an ideal input distribution. For example, we expect that the channel capacity of the pheromone response system in Δ*sst2* cells is lower than that in wild-type cells because of dose-response misalignment; using the channel capacity, we could quantify exactly how much worse in a more "absolute" sense. Likewise, if we choose doses such that they are distributed where the response is not saturated, we expect that small changes in input dose will be more distinguishable by the respective outputs.

Using these metrics allow one to quantitatively compare how well different systems can distinguishably and precisely respond to different inputs, as well as measure how much molecular mechanisms, such as Fus3-mediated negative feedback, affect the ability of systems to transmit information, such as external pheromone concentration.

Supplementary Tables

Table S1. Strains used in this work

Name	Relevant Genotype
ACL379	MATa bar1Δ [10]
ACL387	MATa bar1Δ PRM1Δ::P_{PRM1}-YFP-::his3MX6 [10]
ACL394	MATa bar1Δ PRM1Δ::P_{PRM1}-YFP-::his3MX6 cdc28-as2 [10]
RY1000	MATa bar1Δ ste12Δ::TRP1
RY1130b	MATa bar1Δ dig1Δ::kanMX6 ste12Δ::TRP1 dig1::pP_{DIG1}-DIG1-YFP::ura3 ste12::pP_{STE12}-CFP-STE12::LEU2(3x)
RY1130bPY	MATa bar1Δ dig1Δ::kanMX6 ste12Δ::TRP1 dig1::pP_{DIG1}-DIG1-YFP::ura3 ste12::pP_{STE12}-CFP-STE12::LEU2(3x) PRM1Δ::P_{PRM1}-YFP-::his3MX6
RY1130b	MATa bar1Δ dig1Δ::kanMX6 ste12Δ::TRP1 dig1::pP_{DIG1}-DIG1-YFP::ura3 ste12::pP_{STE12}-CFP-STE12::LEU2(3x) *cdc28-as2*
RY1133b	MATa bar1Δ dig1Δ::kanMX6 ste12Δ::TRP1 dig1::pP_{DIG1}-DIG1-YFP ste12::pP_{STE12}-CFP-STE12::LEU2(3x) kss1::kss1-as2
RY1134b	MATa bar1Δ dig1Δ::kanMX6 ste12Δ::TRP1 dig1::pP_{DIG1}-DIG1-YFP ste12::pP_{STE12}-CFP-STE12::LEU2(3x) fus3::fus3-as2
RY1135b	MATa bar1Δ dig1Δ::kanMX6 ste12Δ::TRP1 dig1::pP_{DIG1}-DIG1-YFP ste12::pP_{STE12}-CFP-STE12::LEU2(3x) fus3::fus3-as2 kss1::hphMX4
RY1135bPY	MATa bar1Δ dig1Δ::kanMX6 ste12Δ::TRP1 dig1::pP_{DIG1}-DIG1-YFP ste12::pP_{STE12}-CFP-STE12::LEU2(3x) fus3::fus3-as2 kss1::hphMX4 PRM1Δ::P_{PRM1}-YFP::his3MX6
RY1137b	MATa bar1Δ dig1Δ::kanMX6 ste12Δ::TRP1 dig1::pP_{DIG1}-DIG1-YFP ste12::pP_{STE12}-CFP-STE12::LEU2(3x) fus3::fus3-as2 kss1::kss1-as2
RY1137bPY	MATa bar1Δ dig1Δ::kanMX6 ste12Δ::TRP1 dig1::pP_{DIG1}-DIG1-YFP ste12::pP_{STE12}-CFP-STE12::LEU2(3x) fus3::fus3-as2 kss1::kss1-as2 PRM1Δ::P_{PRM1}-YFP::his3MX6
RY2005	MATa bar1Δ dig1Δ::kanMX6 ste12Δ::TRP1 ste12::pP_{STE12}-CFP-STE12::LEU2(3x)
RY2013	MATa bar1Δ ste5Δ:YFP-STE5 trp1::pP_{STE5}-YFP-STE5::TRP1 fus3Δ::natMX4 P_{FUS3}::pP_{FUS3}-fus3-as2
RY2024	MATa bar1Δ ste5Δ:YFP-STE5 trp1::pP_{STE5}-YFP-STE5::TRP1 fus3Δ::natMX4 P_{FUS3}::pP_{FUS3}-fus3-as2 sst2Δ::hphMX4
RY2025	MATa bar1Δ dig1Δ::kanMX6 ste12Δ::TRP1 dig1::pP_{DIG1}-DIG1-YFPdark::ura3 ste12::pP_{STE12}-CFP-STE12::LEU2(3x)
RY2026	MATa bar1Δ dig1Δ::kanMX6 ste12Δ::TRP1 ste12::pP_{STE12}-CFP-STE12::LEU2
RY2027	MATa bar1Δ dig1Δ::kanMX6 ste12Δ::TRP1 ste12::pP_{STE12}-CFP-STE12::LEU2 (2x)
RY2052b	MATa bar1Δ prm1Δ::YFP::his3mx6 fus3-as2
RY702	MATa bar1Δ prm1Δ::YFP::his3mx6 fus3Δ::TRP1 kss1Δ::kanMX6
RY700	MATa bar1Δ prm1Δ::YFP::his3mx6 fus3Δ::TRP1
RY2053	MATa bar1Δ prm1Δ::YFP::his3mx6 kss1Δ::kanMX6 fus3-as2
RY701	MATa bar1Δ prm1Δ::YFP::his3mx6 kss1Δ::TRP1
RY2055	MATa bar1Δ prm1Δ::YFP::his3mx6 fus3Δ::TRP1 kss1-as2
RY2073	MATa bar1Δ P_{Act1}-mRFP::LYP1::ura3 prm1Δ::YFP::his3mx6 P_{Prm1}CFP::TRP1
RY2077	MATa bar1Δ ste5Δ:YFP-STE5 trp1::pP_{STE5}-YFP-STE5::TRP1 fus3Δ::natMX4 P_{FUS3}::pP_{FUS3}-fus3-as2 sst2::sst2-T134A

TCY3057	MATa bar1Δ ste5Δ::YFP-STE5 trp1::pP_{STE5}-YFP-STE5::TRP1
TCY3154	MATa bar1Δ prm1Δ::YFP::his5 trp1::pP_{ACT1}-CFP::TRP1

All strains derive from ACL379, a W303 derivative, as described above.

Table S2. Plasmids used in this work

Name	Description	Source
pRY1001	pRS405 P_{STE12}-CFP-STE12	This work
pRY1004	pRS406 P_{DIG1}-DIG1-YFP	This work
pRY1004d	pRS406 P_{DIG1}-DIG1-YFPdark	This work
pRY1006	pBS10 mCherry-hphMX4	This work
pES1002	pRS406 P_{FUS3}-fus3-as2	This work
pES1004	pRS406 P_{KSS1}-kss1-as2-trunc	This work
pGP1001	pRS406 P_{ACT1}-mRFP	This work
pYFP-His3MX6	pFA6a-YFP-His3MX6	Colman-Lerner [3]

Table S3. Nuclear CFP fluorescence intensities

Strain	Median	Standard Error (n~200)
RY1100	82.4	1.5
RY1130b	376.5	6.2
RY2025	403.5	6.6

Table S4. Raw nuclear and background values for FRET analysis of pheromone-stimulated cells

	0 min							3 min							
ID	CC	B_{CC}	CY	B_{CY}	YY	B_{YY}	*F*	CC	B_{CC}	CY	B_{CY}	YY	B_{YY}	*F*	Δ*F*
1	448.755	383.199	781.204	638.155	251.327	195.056	1.287	369.163	338.535	549.408	488.822	226.000	190.059	0.912	-0.375
2	446.347	390.337	784.408	678.410	250.020	196.376	0.922	365.705	334.751	553.023	493.864	228.659	188.145	0.805	-0.117
3	400.143	373.714	681.612	620.429	216.327	191.186	1.359	342.633	323.690	494.041	457.854	202.898	187.456	1.019	-0.339
4	426.327	383.711	751.102	649.024	232.082	193.232	1.472	346.510	327.714	522.041	466.946	216.408	186.564	1.541	0.069
5	420.674	388.315	722.408	644.050	219.143	196.435	1.709	354.531	338.919	518.816	482.610	209.510	190.481	1.204	-0.505
6	422.854	378.159	747.667	645.395	227.958	192.571	1.459	349.681	325.280	529.128	471.128	216.979	186.531	1.242	-0.217
7	412.805	382.460	732.561	655.741	231.756	193.443	1.372	346.313	330.243	520.000	484.570	215.042	187.822	0.933	-0.439
8	416.327	383.659	737.571	647.161	214.959	195.117	2.281	346.286	331.683	510.592	473.206	199.592	188.453	1.798	-0.483
9	419.347	385.927	746.286	664.466	224.796	194.410	1.529	354.776	339.020	529.959	483.785	211.265	187.641	1.585	0.055
10	418.674	384.486	719.265	653.203	225.449	193.877	0.981	349.204	329.034	517.327	470.751	212.918	187.232	1.169	0.188
11	421.143	378.164	737.306	640.393	241.612	192.986	1.189	351.592	323.941	520.612	466.904	225.653	187.105	0.807	-0.383
12	406.429	378.066	638.388	593.596	212.735	190.556	0.666	338.184	327.921	481.449	452.537	204.918	186.012	1.346	0.680
13	422.939	373.440	696.082	592.655	225.898	192.466	1.338	350.857	321.739	507.939	452.033	215.367	187.133	0.944	-0.393
14	421.163	374.863	717.612	620.705	224.429	193.734	1.355	352.367	322.786	514.592	456.019	212.245	187.585	1.084	-0.270
15	401.714	371.420	682.857	611.518	214.612	192.607	1.601	347.694	321.849	504.776	456.460	206.674	187.349	1.017	-0.584
16	409.959	370.018	736.898	626.155	238.898	194.227	1.686	346.327	319.763	536.143	464.455	222.388	187.715	1.496	-0.190
17	412.857	378.766	719.061	624.210	218.327	193.956	2.120	344.878	334.916	507.612	469.702	201.225	188.387	2.480	0.360
18	401.225	373.531	627.796	559.634	214.265	189.305	1.550	345.184	329.969	466.082	434.189	205.225	185.272	0.966	-0.584
19	421.367	369.887	749.000	613.809	214.469	194.177	2.606	357.674	320.647	525.020	462.359	202.245	188.382	1.148	-1.458
20	417.041	376.839	717.122	630.877	240.592	193.480	1.067	355.674	330.074	527.755	475.912	225.837	187.705	0.848	-0.219
21	463.833	409.129	849.625	748.483	234.604	198.129	1.052	365.735	344.492	571.939	532.886	217.796	189.417	0.734	-0.318
22	398.918	366.093	672.102	595.954	213.653	191.384	1.615	327.653	315.382	473.245	438.747	204.143	186.667	1.526	-0.088
23	391.429	365.970	648.592	578.854	224.837	191.490	1.528	332.469	317.494	486.633	442.694	212.694	186.478	1.469	-0.059
24	417.735	371.842	723.408	627.683	238.469	192.842	1.099	345.286	321.438	519.857	464.767	223.204	189.322	1.108	0.008
25	398.020	357.294	669.857	578.881	217.020	191.477	1.571	338.306	311.277	475.694	432.693	204.653	185.861	0.721	-0.850
26	388.367	354.095	651.490	574.947	218.347	190.735	1.385	334.724	314.800	482.276	440.221	197.621	185.876	1.460	0.074
27	399.388	359.727	674.796	582.305	221.531	191.947	1.554	345.816	323.142	491.367	446.991	209.980	186.228	0.945	-0.609
28	375.122	355.985	579.245	540.252	203.918	191.916	1.323	329.694	312.835	440.674	415.589	193.265	187.298	0.837	-0.486
29	387.974	355.886	635.026	573.907	227.821	191.343	0.858	332.936	316.333	472.774	435.000	216.194	186.521	0.961	0.103
30	351.796	335.556	577.571	529.519	210.225	192.259	1.872	312.292	296.159	447.313	408.659	201.292	186.516	1.469	-0.403
31	360.367	338.671	578.980	528.259	213.653	190.553	1.306	315.818	298.293	441.818	407.354	203.818	186.037	0.970	-0.337
32	371.592	341.316	613.571	563.942	216.327	194.129	0.758	323.592	303.897	458.469	425.728	206.286	186.949	0.679	-0.080
33	353.612	335.298	587.857	540.115	210.469	190.817	1.561	311.750	298.615	437.150	405.531	208.950	185.787	1.067	-0.494
34	351.306	333.280	584.837	515.565	228.918	190.956	1.966	308.327	298.577	440.429	404.207	207.204	187.325	1.909	-0.057
35	345.776	329.394	572.776	521.052	215.612	188.723	1.692	304.542	294.407	430.708	401.573	205.479	185.141	1.331	-0.361
36	401.347	375.545	689.408	631.333	206.245	195.317	1.937	333.102	328.007	493.592	458.791	196.898	188.453	4.536	2.599
37	423.429	383.837	781.408	662.473	235.571	194.954	1.988	354.429	327.293	539.469	475.459	221.694	188.452	1.237	-0.752
38	366.102	343.445	618.327	554.246	214.041	191.145	1.829	314.408	304.228	461.939	424.688	203.510	186.505	2.065	0.237
39	359.327	335.801	600.490	541.842	219.816	191.615	1.373	316.646	305.667	453.167	422.644	207.667	186.148	1.279	-0.094
40	399.816	353.444	604.878	519.880	246.694	193.485	0.787	378.816	344.113	563.980	488.263	242.714	192.315	0.989	0.202
41	374.367	350.734	606.857	511.817	228.592	193.219	2.478	378.306	346.427	571.286	505.225	231.286	193.174	0.990	-1.488
42	378.327	360.086	577.816	537.356	214.796	196.681	1.232	377.469	352.495	553.367	511.214	214.959	194.777	0.776	-0.456
43	406.408	360.792	634.980	544.043	235.020	193.827	1.056	392.939	349.280	585.980	505.428	234.816	192.873	0.872	-0.184
44	387.510	350.240	588.551	510.560	228.449	193.890	1.145	379.571	343.640	568.571	485.020	234.184	192.840	1.245	0.100
45	374.143	345.597	581.204	507.415	225.061	193.805	1.524	363.327	337.326	543.469	485.686	226.776	192.636	1.075	-0.449
46	371.061	350.048	586.612	523.172	225.061	195.128	1.700	363.510	344.986	551.612	503.280	230.735	193.989	1.150	-0.550
47	399.286	342.916	572.204	482.785	231.143	191.869	0.714	384.102	337.742	524.939	464.910	227.184	192.425	0.352	-0.362
48	390.939	349.572	605.327	517.873	244.816	194.838	1.023	385.531	340.601	574.735	494.970	243.449	194.205	0.750	-0.273
49	334.225	315.134	479.122	431.768	217.551	192.083	1.290	327.020	311.202	462.041	417.828	218.286	190.847	1.371	0.080
50	361.776	340.975	509.306	463.590	216.612	192.084	1.112	357.000	338.120	487.980	450.172	218.225	191.320	0.848	-0.264
51	376.816	341.028	580.510	502.134	239.388	193.470	1.059	360.563	335.414	546.021	480.175	238.042	192.035	1.204	0.144
52	358.469	333.048	537.959	478.677	213.837	192.836	1.476	352.143	326.685	513.204	459.096	216.163	191.680	1.158	-0.319
53	347.458	339.857	505.583	481.633	205.958	195.857	1.875	350.044	334.671	498.311	468.211	212.533	192.842	0.855	-1.019
54	372.041	339.161	571.694	491.333	223.490	194.416	1.546	367.388	330.416	546.469	471.852	232.306	192.127	0.986	-0.560
55	371.041	337.552	558.041	482.852	229.694	192.372	1.189	356.667	330.645	510.813	458.839	227.042	192.167	0.870	-0.319
56	352.000	341.189	521.750	498.101	212.688	194.797	0.931	348.469	328.687	508.122	470.362	212.408	193.005	0.928	-0.003
57	380.222	341.230	595.000	501.034	237.963	192.638	1.317	360.458	337.971	544.750	483.432	243.167	191.764	1.149	-0.168
58	367.347	336.385	540.041	472.469	233.714	192.495	1.033	355.796	325.964	507.429	446.554	229.857	191.789	0.930	-0.103
59	358.020	329.820	530.122	475.336	223.755	194.977	0.943	348.531	321.219	492.980	447.437	228.531	192.498	0.590	-0.353
60	349.653	326.825	507.694	463.683	222.225	191.976	0.815	329.633	322.092	474.735	443.229	212.367	192.340	1.956	1.141
61	335.225	315.429	482.204	438.821	212.000	192.900	1.223	329.735	308.973	471.429	424.577	219.367	191.220	1.088	-0.135
62	352.939	321.377	536.102	461.956	240.163	194.539	1.131	343.020	314.622	492.674	439.541	232.714	195.378	0.768	-0.362
63	337.612	310.654	487.286	431.083	218.408	191.239	1.091	322.898	305.122	454.041	414.776	210.367	190.654	1.157	0.067
64	346.298	331.844	509.447	481.091	209.234	193.487	0.931	343.510	321.437	494.857	456.349	220.939	191.403	0.652	-0.279
65	399.551	360.589	624.898	538.185	238.429	195.147	1.172	386.327	347.244	585.408	505.977	240.918	195.488	0.967	-0.205
66	399.306	356.102	610.347	523.106	234.061	192.801	1.053	384.980	343.641	570.857	490.945	234.204	193.604	0.952	-0.102
67	389.653	356.612	578.939	522.082	216.204	192.465	0.862	373.245	342.294	537.633	488.625	219.143	192.408	0.638	-0.224

68	350.939	327.538	512.082	459.815	220.531	191.382	1.114	337.306	318.386	473.959	437.587	221.816	191.730	0.739	-0.375
69	368.796	346.793	546.449	486.362	219.204	190.655	1.528	353.604	336.148	510.896	467.526	217.417	191.504	1.227	-0.302
70	373.367	347.957	556.245	500.389	213.918	192.885	1.328	362.388	339.571	527.837	481.728	217.000	193.102	1.007	-0.321
71	362.306	345.986	533.143	497.169	208.020	193.183	1.273	349.551	339.246	509.388	481.116	208.735	192.732	1.407	0.134
72	407.633	356.471	626.041	527.731	238.061	193.912	1.003	398.735	349.779	588.408	509.077	237.878	195.010	0.674	-0.329
73	364.122	341.281	516.388	476.018	207.388	191.994	0.947	357.061	329.988	494.061	445.793	211.449	192.337	0.944	-0.003
74	379.469	349.443	569.898	504.415	221.837	191.779	1.190	367.837	345.097	527.184	489.028	223.837	191.883	0.580	-0.610
75	392.694	345.996	596.857	500.505	233.327	192.824	1.152	378.306	340.645	546.918	478.978	229.837	193.039	0.823	-0.329
76	376.816	344.362	561.674	491.687	222.531	192.623	1.215	362.245	336.693	532.980	468.848	223.980	192.113	1.361	0.146
77	368.102	343.742	553.163	500.526	222.082	192.353	1.060	354.978	336.259	522.761	477.697	219.761	192.796	1.181	0.121
78	356.653	329.324	526.408	452.074	221.408	191.147	1.644	354.020	325.930	497.796	443.434	221.735	190.944	0.903	-0.741
79	350.755	330.524	506.327	456.986	207.571	192.054	1.654	342.225	322.568	484.959	445.658	215.265	192.871	0.946	-0.709
80	350.796	324.018	503.204	442.777	214.429	191.072	1.356	334.347	316.227	470.143	421.939	218.327	190.348	1.344	-0.012
81	358.061	330.528	516.408	464.966	221.163	191.579	0.847	342.796	320.478	485.429	446.096	221.123	191.774	0.674	-0.174
82	353.918	328.956	525.592	464.774	221.653	190.973	1.305	341.878	323.735	488.898	443.589	221.102	190.889	1.168	-0.137
83	347.204	317.840	496.347	445.445	219.674	190.412	0.745	331.245	307.876	465.184	424.060	217.061	191.068	0.730	-0.015
84	379.694	357.881	567.265	525.651	214.959	194.484	0.947	362.082	347.893	530.714	496.626	213.837	194.362	1.206	0.258
85	375.510	352.616	571.592	507.192	220.429	192.227	1.642	366.061	342.000	536.000	484.448	220.204	192.344	1.071	-0.571
86	391.898	355.843	616.122	528.854	223.408	194.384	1.594	371.878	346.587	548.429	503.239	223.633	193.811	0.734	-0.861
87	374.102	349.578	556.041	492.442	216.612	192.915	1.631	361.327	340.900	530.612	474.228	220.612	192.972	1.522	-0.109
88	380.796	351.005	561.796	502.683	223.367	192.661	0.979	379.102	345.240	534.510	483.584	224.898	192.589	0.526	-0.453
89	384.857	343.500	551.796	468.040	232.592	192.330	1.049	369.184	335.055	519.857	447.175	235.306	192.491	1.017	-0.032
90	382.184	342.353	584.959	496.644	232.163	192.747	1.234	362.102	332.824	544.878	474.201	230.388	193.152	1.263	0.029
91	368.122	339.561	556.327	473.365	234.837	192.306	1.569	355.898	332.913	522.592	458.023	236.123	191.523	1.306	-0.263
92	363.816	340.353	544.796	476.804	225.980	192.557	1.598	352.653	331.666	505.857	458.628	224.163	192.272	1.022	-0.576
93	352.082	331.730	506.306	455.682	218.939	191.075	1.280	350.000	323.913	482.347	434.061	219.327	191.163	0.829	-0.451
94	364.980	348.274	545.408	517.026	205.796	194.530	0.863	353.980	337.888	517.633	478.276	207.204	192.388	1.517	0.654
95	373.918	349.526	561.061	511.804	213.612	196.041	1.213	365.714	342.586	530.306	494.320	212.061	195.627	0.671	-0.541
96	385.674	344.882	590.469	505.038	225.367	192.968	1.239	368.959	337.531	537.857	483.164	225.633	192.446	0.730	-0.509
97	369.791	350.081	560.907	511.397	213.442	191.464	1.441	362.029	344.949	529.486	486.521	219.571	190.462	1.169	-0.273
98	383.531	346.280	567.633	491.815	226.000	193.037	1.111	379.857	341.757	530.551	470.324	219.674	192.445	0.699	-0.412
99	373.531	340.470	557.898	479.222	218.429	191.231	1.532	365.184	333.277	523.898	461.378	217.286	190.647	1.061	-0.471
100	379.735	346.839	575.184	515.092	222.082	193.369	0.896	371.225	337.222	538.755	486.992	216.837	193.696	0.645	-0.250
101	370.245	335.822	550.857	481.923	220.592	191.512	1.102	360.204	333.639	523.918	472.708	216.612	191.769	0.970	-0.132
102	363.639	344.952	540.500	499.324	214.917	191.396	1.082	353.532	337.783	511.766	479.157	220.043	190.300	0.786	-0.295
103	359.449	340.217	541.694	493.935	211.225	192.413	1.510	350.857	333.054	517.143	481.262	210.633	192.308	1.011	-0.499
104	369.551	340.098	552.776	493.623	223.000	197.153	1.087	362.980	331.313	529.225	473.399	221.633	194.969	0.842	-0.245
105	366.490	336.124	549.878	484.163	214.551	192.647	1.382	352.898	332.757	523.000	473.493	211.408	193.736	1.567	0.185
106	370.041	335.728	567.469	486.330	229.041	192.481	1.332	361.265	327.875	535.551	467.525	225.531	192.410	1.052	-0.280
107	367.041	335.162	564.163	487.797	227.265	192.437	1.345	362.571	328.937	534.674	464.021	228.347	191.195	1.057	-0.288
108	356.429	331.397	532.918	475.245	223.000	192.629	1.193	349.979	327.367	513.458	458.861	224.500	191.114	1.172	-0.021
109	364.469	336.929	541.367	487.433	217.776	193.000	1.021	354.388	333.593	512.714	467.657	218.592	192.093	1.042	0.021
110	350.510	329.925	495.674	454.833	215.510	192.624	0.943	347.245	320.070	485.286	434.018	216.061	192.436	0.962	0.019
111	375.469	353.512	576.837	517.104	219.878	192.554	1.551	373.571	345.944	541.939	492.602	218.286	192.175	0.819	-0.733
112	371.551	347.762	559.286	501.462	219.225	192.610	1.362	362.592	340.371	518.429	472.668	215.163	192.112	1.050	-0.312
113	394.408	350.969	615.327	520.758	237.878	195.292	1.199	378.674	341.475	556.939	492.058	235.184	193.211	0.710	-0.489
114	374.653	344.799	574.918	502.237	227.469	192.931	1.343	369.367	338.427	562.245	482.865	228.837	192.204	1.448	0.105
115	380.163	345.714	585.714	497.850	228.674	192.245	1.518	362.776	344.484	548.633	485.925	224.939	191.763	1.810	0.293
116	365.612	338.927	537.265	490.484	216.204	193.359	0.825	357.755	330.154	516.204	469.325	213.265	192.739	0.822	-0.003
117	375.265	339.768	562.878	488.208	226.306	191.716	1.128	355.612	329.502	517.837	461.871	215.490	191.676	1.208	0.080
118	356.531	334.393	519.980	471.273	213.980	195.711	1.332	354.041	327.204	509.694	453.622	220.184	193.804	1.109	-0.223
	0 min							3 min							
	CC	B_{CC}	CY	B_{CY}	YY	B_{YY}	F	CC	B_{CC}	CY	B_{CY}	YY	B_{YY}	F	ΔF
mean	380.698	349.908	597.893	528.453	222.907	192.933	1.313	353.388	329.446	513.917	463.819	218.761	190.749	1.102	-0.200
SE	2.362	1.717	7.275	5.968	0.924	0.150	0.033	1.687	1.187	3.178	2.410	0.974	0.251	0.043	0.046
median	374.888	345.991	576.010	507.304	221.592	192.643	1.289	354.214	330.530	518.133	467.592	218.306	191.746	1.018	-0.250
SE	1.906	1.351	5.754	4.751	0.740	0.116	0.025	1.279	0.940	2.508	1.932	0.766	0.213	0.026	0.029

Table S6. Raw nuclear and background values for FRET analysis of unstimulated cells

	0 min							3 min							
ID	CC	B_{CC}	CY	B_{CY}	YY	B_{YY}	*F*	CC	B_{CC}	CY	B_{CY}	YY	B_{YY}	*F*	Δ*F*
1	385.204	361.612	591.347	526.135	208.061	188.618	1.954	382.959	350.740	561.490	506.422	206.408	186.729	0.920	-1.034
2	374.857	353.991	565.612	518.269	202.735	188.000	1.522	368.020	341.204	538.367	487.711	213.265	185.894	0.890	-0.632
3	393.306	358.777	616.082	533.941	224.123	188.112	1.360	375.653	346.190	559.694	497.220	220.776	185.966	1.040	-0.320
4	387.490	353.813	595.204	504.940	229.714	189.874	1.554	373.939	342.168	552.041	478.946	226.551	188.600	1.199	-0.355
5	375.878	351.829	599.204	534.471	200.020	187.995	2.407	361.184	341.133	547.612	492.390	208.163	187.051	1.719	-0.687
6	374.490	357.686	591.449	539.071	215.612	192.442	1.811	362.449	344.606	560.265	504.445	213.327	190.467	1.889	0.078
7	375.469	343.684	567.082	495.640	216.837	188.070	1.322	359.469	332.509	532.878	471.912	215.388	186.956	1.238	-0.084
8	376.694	351.420	577.102	527.473	223.796	189.187	0.832	363.041	337.901	546.510	494.969	222.857	187.957	0.900	0.068
9	384.918	354.550	588.449	523.328	217.225	188.389	1.185	361.571	340.777	532.796	489.475	212.286	187.569	1.003	-0.182
10	381.347	350.869	583.612	528.312	210.143	188.238	0.972	368.898	339.121	551.449	489.390	209.000	186.440	1.257	0.284
11	362.694	346.892	547.816	514.120	198.878	189.605	1.491	355.633	336.109	528.429	487.312	198.327	188.126	1.544	0.053
12	383.571	355.517	568.020	506.170	216.796	187.478	1.188	367.061	347.246	530.816	473.723	213.816	186.446	1.609	0.421
13	364.571	351.104	554.041	520.425	206.714	188.293	1.288	347.245	340.274	516.959	483.132	204.571	186.679	2.411	1.123
14	374.286	346.278	590.225	548.439	199.020	188.416	0.816	363.000	335.166	524.204	489.492	195.796	186.873	0.454	-0.362
15	340.551	312.418	495.490	435.989	214.633	185.813	1.111	327.265	301.195	463.469	407.695	213.061	184.847	1.105	-0.007
16	397.796	362.188	614.327	538.096	229.449	189.872	1.092	379.551	348.338	572.184	496.240	230.755	187.982	1.233	0.141
17	377.755	355.547	579.143	532.011	208.408	189.636	1.231	368.408	344.929	551.531	503.779	210.857	188.025	1.058	-0.173
18	380.959	352.221	593.286	510.732	222.163	188.541	1.741	362.980	344.531	554.592	485.218	218.694	187.019	2.114	0.374
19	374.939	352.045	586.878	526.315	219.633	190.245	1.461	364.000	339.036	552.571	495.032	220.531	189.023	1.170	-0.291
20	387.571	351.543	587.469	531.511	229.612	189.525	0.534	366.265	339.395	550.204	503.691	228.449	188.476	0.608	0.074
21	387.816	353.109	603.939	528.956	226.796	192.456	1.177	368.082	340.559	565.551	490.907	229.327	190.163	1.444	0.267
22	361.816	339.947	538.429	496.435	214.755	189.512	0.866	352.674	329.420	512.510	469.179	213.204	188.099	0.841	-0.025
23	369.633	336.281	549.551	479.174	226.674	190.010	1.068	351.469	325.338	509.571	450.414	221.571	189.145	1.144	0.075
24	346.743	319.578	494.543	445.858	214.943	188.466	0.813	331.125	314.188	458.646	424.878	206.167	187.569	0.958	0.145
25	386.490	353.575	601.102	520.593	230.061	193.707	1.385	376.837	346.663	571.918	498.757	228.857	193.959	1.334	-0.051
26	387.408	355.173	606.449	529.494	241.123	194.078	1.157	375.225	352.361	574.571	508.876	242.347	193.070	1.283	0.126
27	387.408	356.464	567.878	507.740	219.674	192.862	1.024	371.837	357.736	535.714	490.442	214.163	193.258	1.824	0.800
28	379.980	350.127	583.592	517.376	222.245	193.558	1.253	365.735	341.840	551.225	493.928	214.816	194.103	1.512	0.259
29	378.102	355.884	584.000	532.581	226.755	195.643	1.119	370.551	348.112	554.674	511.172	225.878	194.522	0.803	-0.317
30	372.102	348.385	552.061	492.375	213.714	194.250	1.685	357.878	337.720	521.612	470.970	209.408	193.810	1.731	0.045
31	385.061	359.007	591.592	519.785	229.531	192.556	1.482	375.918	353.608	553.776	495.554	225.388	192.213	1.328	-0.154
32	415.531	368.723	634.061	533.704	230.327	193.000	1.292	392.612	356.988	577.755	497.364	223.102	193.085	1.380	0.088
33	391.041	348.143	595.102	503.621	232.694	193.424	1.194	377.612	342.418	553.388	488.450	235.327	192.718	0.777	-0.417
34	378.429	347.145	564.612	497.829	226.367	192.829	1.106	366.980	342.768	538.776	480.387	221.918	192.873	1.298	0.192
35	370.633	339.016	540.857	478.862	221.041	193.598	1.042	367.082	331.656	520.306	458.984	222.776	192.318	0.799	-0.243
36	372.735	339.175	566.061	491.221	236.123	193.750	1.104	352.816	332.875	524.204	472.109	226.592	193.962	1.268	0.165
37	363.612	331.323	502.143	459.474	209.735	191.827	0.445	346.521	331.406	482.875	450.042	209.688	191.769	1.086	0.641
38	353.041	325.674	510.939	457.085	213.041	190.922	1.088	344.364	326.873	481.250	448.168	212.091	190.839	0.818	-0.270
39	345.469	321.141	510.714	450.714	217.306	191.876	1.444	337.000	326.840	489.653	452.512	215.306	192.642	1.785	0.341
40	344.469	321.142	496.225	446.237	221.367	191.721	1.023	336.551	317.284	473.184	430.098	217.857	192.404	1.084	0.062
41	376.531	353.505	553.490	513.612	213.776	192.422	0.770	371.367	351.332	545.735	495.567	213.878	192.455	1.464	0.694
42	389.204	355.686	594.408	531.943	222.837	194.976	0.958	380.674	345.466	569.143	498.505	228.674	193.976	1.024	0.066
43	389.286	351.946	585.286	511.446	231.367	195.681	1.010	368.612	342.063	547.755	485.094	227.571	194.390	1.226	0.215
44	386.225	351.613	594.449	514.382	229.306	193.260	1.297	372.625	349.688	561.646	500.400	227.167	193.044	1.378	0.081
45	376.633	347.846	527.531	483.809	212.245	192.735	0.642	374.939	346.473	514.878	467.479	208.857	192.467	0.890	0.247
46	363.612	340.375	528.327	475.132	212.102	192.996	1.433	347.041	333.984	487.714	456.289	207.102	192.530	1.341	-0.092
47	355.918	328.774	523.184	467.540	214.898	191.429	1.140	342.469	324.292	493.755	451.128	215.041	190.620	1.169	0.029
48	349.388	325.243	518.163	462.847	223.633	192.431	1.144	340.286	322.596	499.388	445.618	223.123	191.544	1.534	0.390
49	350.429	324.214	509.776	451.632	228.061	193.669	1.072	343.449	321.347	491.878	431.044	231.429	192.871	1.334	0.262
50	426.633	403.638	631.837	577.731	212.490	194.669	1.548	365.796	351.892	493.980	464.682	208.245	191.554	1.020	-0.529
51	440.429	401.450	711.735	619.932	221.878	197.219	1.716	374.633	344.922	537.531	484.654	216.735	193.148	0.886	-0.830
52	443.857	396.102	701.143	606.537	241.633	196.041	1.014	368.592	343.218	539.265	483.612	229.633	193.905	1.014	0.000
53	456.939	396.578	723.612	629.667	229.306	197.824	0.784	373.163	337.240	543.592	477.070	217.694	192.450	1.028	0.244
54	462.306	399.269	754.367	631.050	252.694	199.454	1.051	385.041	340.820	584.367	491.360	243.898	194.790	1.056	0.005
55	427.408	404.091	688.082	638.882	223.327	198.839	1.093	365.638	349.180	530.894	499.131	221.319	194.612	0.738	-0.355
56	444.939	401.520	727.674	640.834	241.367	198.983	1.022	374.551	342.841	553.490	494.271	223.592	195.835	0.938	-0.084
57	437.918	387.974	713.857	623.621	244.347	198.451	0.852	369.122	335.497	551.408	493.222	227.163	195.092	0.758	-0.094
58	431.551	397.214	706.469	627.398	227.674	199.265	1.443	368.306	339.963	543.898	484.833	221.265	194.139	1.118	-0.325
59	448.918	402.352	736.755	621.704	251.347	198.396	1.389	370.980	353.373	557.939	489.381	235.367	193.861	1.891	0.503
60	441.041	405.972	712.367	660.657	230.184	202.662	0.547	371.265	349.634	551.510	507.112	223.367	197.652	0.974	0.428
61	435.633	395.867	687.776	619.113	226.796	199.993	0.897	371.429	347.384	535.674	487.974	225.265	194.252	0.875	-0.022
62	415.490	391.594	664.939	610.867	219.000	198.839	1.386	353.225	339.878	518.490	476.942	219.123	193.385	1.529	0.143
63	433.020	396.571	713.388	634.445	240.878	198.119	1.086	362.531	340.581	537.816	491.186	229.776	194.347	0.893	-0.193
64	439.041	394.495	716.367	626.579	244.123	197.192	0.999	370.652	340.843	547.891	488.443	229.696	193.231	0.908	-0.091
65	429.367	394.908	688.980	623.739	224.000	199.482	1.071	370.265	340.395	538.143	485.554	216.225	195.241	0.919	-0.151
66	449.714	396.755	675.429	582.665	234.449	195.463	0.888	372.633	345.160	512.796	463.723	224.469	192.362	0.736	-0.151
67	438.306	395.759	714.755	623.139	226.306	199.856	1.475	371.347	343.868	548.204	490.989	219.959	195.028	1.147	-0.329

68	423.653	393.673	664.286	595.176	234.041	195.859	1.165	356.755	341.434	514.980	467.137	221.510	192.781	1.557	0.392
69	438.592	402.722	697.674	627.406	224.571	198.675	1.140	380.735	361.091	543.367	498.678	218.796	194.678	1.160	0.019
70	423.714	397.942	689.265	627.916	221.694	197.922	1.448	362.041	340.173	530.429	484.927	216.959	193.660	1.057	-0.391
71	438.878	394.811	707.857	626.430	244.102	198.739	0.845	368.653	338.267	556.163	482.429	232.123	194.604	1.293	0.447
72	428.490	388.784	704.490	608.505	233.388	195.926	1.470	360.347	336.934	535.939	476.563	222.551	192.797	1.371	-0.098
73	430.245	391.661	694.469	607.102	226.143	197.932	1.490	360.714	336.659	524.327	477.259	218.898	193.659	0.944	-0.547
74	421.980	388.387	664.980	602.405	218.286	197.064	1.098	355.204	339.729	506.449	471.362	212.857	193.390	1.139	0.041
75	436.204	398.810	718.653	621.357	234.816	200.147	1.674	365.755	355.678	538.306	495.405	226.306	197.426	1.930	0.256
76	403.000	378.983	589.939	553.122	214.082	197.483	0.653	342.082	322.820	458.857	430.702	208.061	193.590	0.544	-0.109
77	412.816	376.694	664.755	579.536	228.082	195.639	1.445	339.000	333.582	500.000	451.870	219.082	192.022	3.532	2.087
78	404.796	377.943	655.429	592.472	221.082	198.435	1.475	343.204	327.715	502.714	461.220	215.000	194.086	1.453	-0.021
79	399.388	369.273	639.265	553.885	234.082	195.202	1.624	338.143	321.196	474.612	435.709	223.735	192.064	0.955	-0.669
80	413.735	366.565	647.204	558.848	229.980	195.674	1.036	341.653	317.352	482.571	431.077	220.755	192.769	1.052	0.016
81	379.347	356.177	584.571	520.281	219.367	195.140	1.745	326.225	310.568	447.939	411.968	208.816	192.574	1.284	-0.462
82	376.796	350.971	546.735	499.298	218.571	193.789	0.864	316.511	300.844	422.723	395.852	207.192	190.203	0.696	-0.168
83	407.674	374.628	621.061	545.883	228.184	195.964	1.301	345.653	328.690	479.306	437.379	219.225	192.440	1.179	-0.122
84	383.531	353.525	610.143	530.110	240.592	194.655	1.356	323.735	306.159	466.184	415.692	231.674	191.482	1.245	-0.110
85	373.939	351.853	590.367	531.880	224.796	197.103	1.481	327.102	305.056	460.388	413.207	216.204	193.430	1.132	-0.349
86	446.490	401.451	704.143	614.829	245.204	195.988	0.950	370.347	347.405	550.939	489.789	235.245	192.321	1.225	0.275
87	432.245	396.061	685.020	608.133	226.571	196.449	1.244	358.122	339.933	528.327	476.207	221.061	192.311	1.492	0.248
88	438.429	400.231	728.204	638.945	242.388	199.110	1.265	363.612	349.939	555.714	504.700	230.347	195.050	1.706	0.441
89	436.837	404.816	747.225	660.547	243.510	198.689	1.451	367.163	354.415	578.878	527.156	232.143	194.068	1.775	0.324
90	411.102	389.686	684.980	618.708	221.510	199.527	2.077	348.714	335.374	525.367	481.390	214.837	194.795	1.882	-0.195
91	398.367	352.643	605.592	519.618	228.490	192.739	1.007	384.735	347.147	570.000	496.569	227.225	192.237	0.999	-0.008
92	391.980	356.081	582.755	539.893	220.000	195.980	0.249	378.327	356.419	557.592	510.703	216.469	196.871	1.216	0.967
93	358.633	346.122	540.225	498.595	202.571	194.466	2.904	347.148	343.491	509.370	479.322	200.630	194.328	5.505	2.601
94	370.204	355.457	552.225	515.299	211.306	195.000	1.440	356.918	344.900	514.531	485.490	207.653	194.594	1.368	-0.071
95	374.265	348.628	570.755	519.881	215.388	194.408	1.099	369.204	342.383	531.633	495.104	207.245	195.374	0.559	-0.540
96	379.383	348.217	560.277	506.901	235.106	194.882	0.636	354.367	345.873	519.755	481.360	228.245	194.147	1.762	1.126
97	375.327	347.306	598.000	524.945	235.367	195.630	1.358	368.612	348.000	561.531	502.204	233.959	195.363	1.380	0.022
	0 min							3 min							
	CC	B_{CC}	CY	B_{CY}	YY	B_{YY}	*F*	CC	B_{CC}	CY	B_{CY}	YY	B_{YY}	*F*	ΔF
mean	396.718	364.891	614.849	546.838	224.445	194.134	1.220	361.019	338.684	528.525	477.063	219.681	192.036	1.279	0.059
SE	3.132	2.546	7.062	5.930	1.170	0.384	0.040	1.546	1.253	3.372	2.665	0.951	0.297	0.062	0.051
median	387.408	355.547	594.449	531.511	224.123	194.408	1.165	365.735	340.820	535.939	485.094	219.959	192.769	1.170	0.016
SE	2.708	2.215	6.017	5.044	0.924	0.319	0.029	1.234	0.924	2.686	2.059	0.771	0.237	0.036	0.033

Supplementary Figures

Figure S1. An operational model of multi-step pharmacological agonism

Figure shows an operational model of how an agonist (A) causes an effect (E). All binding reactions are mass-action based. Agonist binds to a receptor (R) to form an agonist-receptor complex (AR). This complex then binds to a "transducer", forming an active agonist-receptor-transducer complex (ART). The effect is then proportional to the amount of ART. Black and Leff [24] showed that the magnitude of the maximal effect (i.e., the effect as the concentration of A approached infinity) approaches zero as the EC50 of the dose-response for agonist-receptor binding approaches the EC50 of percentage maximal ART complex formed as a function of agonist concentration. See Supplementary Information S8 for a more detailed discussion.

Figure S2. Correction of Gpa1-Ste18 loss of FRET.

Shown are raw FRET values measured for RY2062, a derivative of a CFP-Gpa1/ Ste18-YFP FRET reporter strain developed by Yi et al. [26]. We define FRET value F in Supplementary Information S2.4. Due to differential photobleaching of acceptor and donor fluorophores after exposures for each timepoint, there is a pheromone-independent drop in F as a function of number of timepoints. We fit a 3rd order polynomial to the timecourse of F measured in unstimulated cells (gray circles). We then subtracted this value from each of the other timecourses, corresponding to different stimuli, to produce corrected membrane recruitment values. We then normalized this corrected Gpa1-Ste18 loss of FRET values as described in specific figure legends.

Figure S3. YFP-Ste5 membrane recruitment reporter controls and analysis.

a) Redistribution of YFP fluorescence occurs in all cells. Top panel: brightfield image. Bottom panel: change in fluorescence intensity in RY2013 cells after 30 seconds of pheromone stimulation. Grey is no change, white indicates maximal increase in fluorescence, and black indicates maximal decrease in fluorescence (calibration bar indicated in upper right of lower panel). Cells were taken from an asynchronous, exponentially growing culture, where we expect approximately 10-20% of the cells to be in a cell cycle position in which there is no transcriptional response to pheromone [27]. However, we see a redistribution of fluorescence in essentially all cells, suggesting there is not a significant effect of cell cycle position on this initial, rapid phase of Ste5 membrane recruitment, in contrast to what is observed at longer timescales [28]. White scale bar in upper right of top panel is approximately 5 μm.

b) Pheromone stimulation causes a redistribution of YFP fluorescence within seconds. Shown is a image stack showing the difference in fluorescence intensity between the time indicated in the upper right of

each sub-panel and time t=0 (before pheromone stimulation). White scalebar is upper left bottom panel is 5 μm.

c) Redistribution of fluorescence corresponds to recruitment of YFP-Ste5 to the cell membrane and depletion from the cell interior. Leftmost column shows brightfield images of cells. Second and third columns are YFP fluorescence images of RY2013 cells at 0 and 30 seconds after pheromone stimulation, respectively (normalied as described in Supplemental Information). Rightmost column shows the change in fluorescence between the column 3 and 2; white is maximal increase, and black is maximal decrease (calibration bar at bottom of panel). (Top row) YFP-Ste5 cells stimulated with pheromone showed depletion of fluorescence from the cell interior and accumulation at the membrane. (Middle row) Without pheromone treatment, there was no redistribution of YFP fluorescence in cells expressing YFP-Ste5, indicating the fluorescence redistribution is pheromone-dependent. (Bottow row) Fluorescence redistribution in YFP channel reflected movement of YFP-Ste5; in cells with unlabelled Ste5 (ACL379) treated with pheromone, there was no redistribution of fluorescence. Scale bar (white) in top left panel is approximately 5 μm.

d) Ste5 membrane recruitment after pheromone stimulation quickly peaked (<=20 seconds). Cells stimulated with 100 nM pheromone (cyan triangles, n=361) showed an increase in median (+/- S.E.) corrected membrane recruitment (corrected fractional change in total membrane fluorescence, scaled to peak value observed for pheromone treated cells, see Supplementary Materials for details) relative to untreated cells (black circles, n=223).

e) Correction of Ste5 recruitment. Shown are fractional changes in total membrane fluorescence since time 0 (discussed further in Supplementary Information). Due to photobleaching, there is a small reduction in YFP fluorescence during each exposure. The photobleaching was approximated by a double exponential, fit to membrane recruitment values calculated for unstimulated cells (gray triangles). We subtracted this value from each of the other data conditions to produce corrected membrane recruitment values, which we then normalized as described in specific figure legends.

f) Normalized histograms of membrane recruitment values for stimulated (solid line) and unstimulated (dotted line) cells at 20 seconds. Distributions are significantly different ($p<0.00001$, KS test).

For Fig. S3, we calculated difference images in panels a, b, and c using ImageJ [18]. We first subtracted mean background values from beginning and ending time point images. We then scaled the image from the end time point to compensate for photobleaching (~2.4% per 0.25 sec exposure), as calculated from the decrease over many exposures in mean YFP signal from cells not stimulated by pheromone. Then

we performed a per-pixel subtraction of the time zero image from the end time point image. We adjusted the pixel intensity display scale to extend from maximal increase (white) to maximal decrease (black), centered on zero change (gray). We did not enhance the contrast of the images by any other processing.

Figure S4. Quantitative immunoblotting of Fus3 phosphorylation levels.

a) Representative scans of immunoblots used to quantify Fus3 and Kss1 phosphorylation levels (see Supplementary Information 3). Image shows two panels representing different scan wavelengths from a single gel. Upper panel: total Kss1 (doublet) and total Fus3; bands as indicated by arrows on the right (680 nm channel). Lower panel: Kss1-P and Fus3-P, phosphorylated on their respective activation loop residues; bands as indicated by arrows on the right (800 nm channel). We indicate time after stimulation after stimulation above panels. M, lane containing molecular weight markers. In immunoblots of otherwise-isogenic deletion strains, there was no significant fluorescence above background at these band positions (data not shown), indicating fluorescence integrated at bands represented signal specific to the probed epitope.

b) Dynamics of Fus3 and Kss1 phosphorylation were similar. Figure shows unscaled mean (+/- SE, n=3) ratio of phosphorylated MAPK to total MAP, as measured from bands from multiple blots as shown in panel (a). Panel shows Fus3 (green triangles) and Kss1 (open black squares) for RY1130b cells treated with 100 nM pheromone at 0 minutes. Kss1 phosphorylation dynamics were consistent with previously-published data [29]. We are unaware of any published data on Fus3 phosphorylation dynamics at or near the time resolution of the present work.

c) Fus3 phosphorylation dynamics do not require additional protein synthesis. Shown are mean (+/- SE, n=3-4) relative Fus3 phosphorylation levels for ACL387 cells stimulated with 100 nM pheromone at time 0, either with (open green squares) or without (filled black circles) simultaneous treatment with 50 μg/ml cycloheximide (CHX), indicating change of Fus3 phosphorylation levels did not depend on additional protein translation.

Figure S5. Characterization of Dig1-Ste12 FRET strain (RY1130b)

a) Growth arrest dose response of RY1130b was similar to that of parent strain ACL379 (ACL379 Δ*ste12* shown as a negative control). Shown are spots of different numbers of cells from exponentially growing cultures, calculated assuming $1.7X10^7$ cells/OD_{600nm}/ml (1 cm cuvette path length): 1000, 100, and 10 cells from top to bottom of each sub-panel. We spotted cells from three strains on plates containing various concentrations of pheromone, as shown, and imaged plates after 48 hours at 30 deg.

b) Dose-response of total system output from Prm1-YFP transcriptional reporter [10] in FRET strain (RY1130bPY) had same EC50 but higher absolute response compared to ACL387 (derived from ACL379, parent of FRET strain). We stimulated cells with varying concentrations of pheromone for 1.5 hours and then treated with 50 μg/ml cycloheximide for an additional 4 hours to allow for fluorophore maturation. We then quantified median total YFP fluorescence per cell. Relative to the levels of YFP system output, total YFP fluorescence from nuclear Dig1-YFP was low (~1-10% of total) and do not strongly correlate with total YFP output (data not shown) and thus do not affect the normalized dose response curve for RY1130bPY.

c) Quantification of CFP-Ste12 and Dig1-YFP levels. Shown are mean +/-SE (n=4-5) CFP-Ste12 and Dig1-YFP protein levels, relative to levels measured for RY1130b (FRET strain), for RY2025 (FRET strain with YFPdark, see Supplemental Information S5), RY1100 (*Δdig1Δste12*), RY2026 (*Δdig1*, 1x *CFP-STE12*), RY2027 (*Δdig1, 2x CFP-STE12*), and RY2005 (*Δdig1, 3x CFP-STE12*). Strains RY2026, RY2027, and RY2005 show discrete increases in amount of protein, consistent with each strain having an additional pRY1001 integrant. Since we do not observe any protein levels below the level of RY2026 for multiple assayed transformants (data not shown), we conclude that this corresponds to a single integrant. RY1130b (FRET strain) is thus consistent with carrying three copies of pRY1001.

Figure S6. FRET data collection protocol

a) Schematic of image splitter. The sample image is passed through an image splitter prior to imaging to split the image into emission wavelength ranges optimized for CFP and YFP emission (480 +/- 15 nm and 525 +/- 30 nm, respectively). In this example, light emitted by a cell exposed to light wavelengths optimized for CFP excitation ("CFPex", 435 +/- 20 nm) first is split by a dichroic mirror (diagonal line in box) into light with wavelengths shorter than 505 nm (green arrow in box) and longer than 505 nm (pink line within box). Emitted light with wavelengths shorter than 505 nm then passes through a filter optimized for detection of CFP emission (cyan rectangle) to produce a CFP emission image ("CFPem",

cyan arrow); likewise, light longer than 505 nm passes through a filter optimized for YFP detection (yellow rectangle) to produce a YFP emission image ("YFPem", yellow arrow). CC indicates CFP excitation/CFP emission wavelengths, and CY indicates CFP excitation/YFP emission wavelengths. See Supplementary Information 2.4 for more details.

b) Image analysis for FRET quantification. Each image is split by an image splitter (as described in a). Top row: brightfield images. Middle row: YFP excitation light images. Bottom row: CFP excitation light images. Left column: raw image; fluorescence intensities calibration bars are in upper right panels. Right column: imaged after being processed and marked by CellID 1.0 [4]. There are four general steps in FRET calculation. 1) (Top row) We identify cell boundaries in both emission channels using defocused brightfield images [4]. 2) (Middle row) We then find the positions of nucleii by looking for peaks of fluorescence within cell boundaries in the YFP excitation/YFP emission image section (bottom of middle row, marked "YY"). At this point, we also extract the observed YY nuclear intensity and cellular background for each cell (see Methods and Supplementary Information 2.4 for details). 3) (Bottom row) We transfer locations of cell borders (indicated by white boundaries in right column) and nucleii onto both CFP excitation/CFP emission ("CC") and CFP excitation/YFP emission ("CY") channels. We then extract CC and CY nuclear intensities and cellular backgrounds for each cell. 4) (Not illustrated) We calculate the FRET value (F) for each cell as described in the Supplementary Information. A similar process is used to measure membrane-region FRET for the Gpa1-Ste18 FRET reporter, except that we use the brightfield image to identify pixels in the image corresponding to membrane-proximal regions and calculate per-cell average FRET values for the membrane regions.

Figure S7. Dig1-Ste12 FRET controls

a) Uncorrected median (+/- S.E.) FRET values over time (F, see Supplementary Information) for reference Dig1-Ste12 FRET reporter strain (RY1130b). Panel shows data presented in Fig. 3d before scaling and baseline correction. Median FRET values for untreated cells (black circles) stays relatively flat, and cells stimulated with 100 nM pheromone (open red triangles) show a relative loss of FRET that peaks in absolute magnitude about 3 minutes after pheromone stimulation.

b) Loss of FRET did not require translation. Loss of FRET measured in pheromone-stimulated cells (filled triangles, n=369) occurred with same rapidity in cells also treated with cycloheximide to block translation (open triangles, n=381). There was little loss of FRET in cells not stimulated with pheromone (filled circles, n=325) and cells treated only with cycloheximide (circles, n=382).

c) Pheromone-stimulated loss of FRET required Ste5. Panel shows measured median (+/- SE) time courses of FRET for cells lacking Ste5 (RY2019), and found no significant difference between cells stimulated with 100 nM pheromone (open red triangles, n=184) and unstimulated cells (black circles, n=218).

d). Loss of FRET required MAP kinase activity. Panel shows median FRET (+/- SE) of cells bearing inhibitor-sensitive alleles of both *fus3* and *kss1* (RY1137b). Cells stimulated with 100 nM pheromone at 0 seconds (open red triangles) showed a loss of FRET over time similar to cells with native Fus3 and Kss1 (panel a). Cells stimulated with pheromone at 0 seconds followed by 10 μM 1-NM-PP1 inhibitor at 4 minutes and 40 seconds (indicated by black arrow) showed a rapid gain in FRET after inhibitor treatment (blue squares, n>100). For reference, panel also shows median FRET values for untreated cells (solid black line) and for cells treated only with inhibitor (dashed line). For cells treated with inhibitor (blue squares and dashed line), FRET levels approached a value higher than that for unstimulated cells, consistent with the idea that inhibition of MAP kinase activity inhibits basal system signal present in the absence of pheromone [30-36]

e) Distribution of FRET values from single cells after treatment with pheromone. Panel shows FRET values calculated for cells before (black) and after (red) 2.5 min of pheromone stimulation. The distributions are significantly distinct ($p<0.00001$, KS test).

Figure S8. Ribonuclease protect assay measurement of *FUS1* mRNA levels

Raw phosphorimaging scan from ribonuclease protection assay to measure induced *FUS1* mRNA levels. Arrows on the left indicate vertical positions of bands corresponding to *FUS1* probe and *ACT1* probe (used as a loading control). Numbers on top indicate time after pheromone stimulation in minutes. Marker lanes are labeled M.

Figure S9. *fus3-as2* and *kss1-as2* are functional alleles and are inhibited by 10 μM 1-NM-PP1.

a) Mean (+/- SE) total system output, measured using fluorescent protein reporter gene expression, for indicated strains (n>100 for each) after 1 hour of stimulation by100 nM pheromone. *fus3-as2Δkss1* cells produced approximately 75 % the total system output as *FUS3Δkss1* cells. Similarly, *Δfus3 kss1-as2* cells produced about twice the total system output as *Δfus3 KSS1* cells. Signaling in *FUS3Δkss1* cells is higher than wild-type cells due to loss of transcriptional inhibition by Kss1 [37].

b) Signaling in *fus3-as2* and *kss1-as2* is inhibited by 10 μM 1-NM-PP1. Shown are mean (+/- SE) total system output for indicated strains (n>100 for each) after 1 hour of stimulation by pheromone. We

observed a slight signal increase in cells without inhibitor-sensitive proteins when they were treated with inhibitor.

Figure S10. RY2062 G-protein FRET strain show *fus3-as2* halo assay phenotypes

We plated $1x10^6$ cells of TMY101 (parent G-protein FRET strain) and RY2062b (TMY101 *fus3-as2*) on YAPD or YAPD + 100 nM pheromone plates, and placed a filter paper disc with 3 µl of 1 mM pheromone (top row), 5 µl of 10 mM 1-NM-PP1 (bottom row), or both (middle row). The *fus3as2* derivative strain (RY2062b) showed an arrest halo around the pheromone-treated disc and a diminished halo around the pheromone+inhibitor treated disc, indicating inhibitor-dependent suppression of pheromone-induced growth inhibition. Likewise, there is a halo of growth around the inhibitor-treated disc on the YAPD+pheromone plate. The small zone of growth arrest immediately adjacent to the borders of discs treated with inhibitor is due to cell death from high concentrations of 1-NM-PP1, presumably due to non-specific inhibition of other essential kinases. Control parent strain (TMY101) showed similar growth arrest halos around discs treated with pheromone and pheromone plus inhibitor, and essentially complete growth inhibition on YAPD+pheromone plates.

Figure S11. Sst2-T134A mediates wild-type levels of growth arrest and is present at levels similar to wild-type Sst2

a) Halo assays of *SST2, sst2*, and *sst2-T134A* (RY2064, RY2065, and RY2066, respectively). 100 µl of cells (OD_{600nm}=1.0) were spread on YPD plates, a filter paper disc was placed on the plate, and 3 µl of 1 mM pheromone was dropped onto the filter. Plates were then incubated for 24 hours. *sst2-T134A* cells (bottom) produced a growth-arrest halo very similar to that of *SST2* cells (top).

b) Quantification of average abundance of wild-type and mutant Sst2. We compared levels of Sst2, relative to levels of a pheromone-insensitive protein (PGK1), in *Δsst2* cells (RY2024), *SST2* cells (RY2013), and *sst2-T134A* cells (RY2077) using quantitative immunoblotting (n=3; started with n=5 and trimmed high and low extreme values). Bar heights indicates mean values, and error bar ends indicate high and low values.

Figure S12. Fus3 phosphorylation dose response after 15 minutes of pheromone stimulation is not altered by inhibition of Cdc28.

Mean dose-response of Fus3 phosphorylation after 15 minutes of pheromone stimulation for asynchronous, exponentially growing cells carrying analogue-sensitive Cdc28, *cdc28-as2* (ACL394, see

[10]), which is inhibited by 5-10 μM 1-NM-PP1 . Figure shows normalized and baseline-subtracted mean +/- SE (n=3-4) values of Fus3 phosphorylation for cells treated with pheromone alone (black circles) and pheromone with inhibitor (open green diamonds). The overlapping dose responses indicated there was little influence of cell cycle position-dependent inhibition of pheromone response on measured Fus3 phosphorylation dose-response for the timescale of experiments (0-15 minutes following pheromone stimulation) presented in this work; effects have been seen for dose-responses of total system output on the timescale of 1-3 hours (see Fig. S4 in [10]).

Figure S13. No desensitization of Fus3 phosphorylation levels during first 30 minutes of pheromone response

Panel shows mean (+/- SE; n=3-5) ratios of phosphorylated Fus3 to total Fus3 in RY1130b cells. After stimulating cells, starting at 0 min, with 0.1 nM pheromone (low pheromone, open green squares), we further stimulated, starting at 16.5 min, with 10 nM pheromone (black arrow indicates time of super-stimulation). Super-stimulated cells responded with another signal (super-stimulated cells, filled green squares) which peaked within 4-5 minutes and reached a plateau amplitude similar to signal from cells initially treated with high, 10 nM pheromone (open black triangles). In Y-axis, we scaled all time courses to plateau signal level (at 16.5 min) for cells stimulated with low pheromone. The lack of adaptation suggests that the system continuously measures and transmits information about external pheromone dose (i.e., receptor occupancy) in terms of the magnitude of the intracellular signal.

Figure S14. Fus3-mediated negative feedback reduces output dynamic range by 50%.

Fus3-mediated dose-response alignment did not drastically reduce dynamic range of downstream responses, in contrast to tuning parameters in a feedback-free multi-step sequential system to achieve dose-response alignment (see Supplementary Information 8). Shown are Fus3 phosphorylation levels, relative to peak levels for uninhibited cells, for cells treated with pheromone in the absence (open green circles) or presence (black circles) of inhibitor.

References

1. **Ausubel, F.M., Brent, R., Kingston, R.E., Moore, D.D., Seidman, J.G., Smith, J.A. et al. *Current protocols in molecular biology*. (John Wiley & Sons, Inc., New York, N.Y., 1987-2006).**
2. **Guthrie, C. and Fink, G.R. *Methods in enzymology, guide to yeast genetics and molecular biology*. (Academic Press, San Diego, California 92101, 1991).**
3. **Colman-Lerner, A., Chin, T.E., and Brent, R. Yeast cbk1 and mob2 activate daughter-specific genetic programs to induce asymmetric cell fates. *Cell* 107, 739-750 (2001).**
4. **Gordon, A., Colman-Lerner, A., Chin, T.E., Benjamin, K.R., Yu, R.C., and Brent, R. Single-cell quantification of molecules and rates using open-source microscope-based cytometry. *Nat Methods* 4, 175-181 (2007).**
5. **Goldstein, A.L. and McCusker, J.H. Three new dominant drug resistance cassettes for gene disruption in saccharomyces cerevisiae. *Yeast* 15, 1541-1553 (1999).**
6. **Baudin, A., Ozier-Kalogeropoulos, O., Denouel, A., LaCroute, F., and Cullin, C. A simple and efficient method for direct gene deletion in saccharomyces cerevisiae. *Nucleic Acids Res.* 21, 3329-3330 (1993).**
7. **Longtine, M.S., McKenzie, A., III, Demarini, D.J., Shah, N.G., Wach, A., Brachat, A. et al. Additional modules for versatile and economical pcr-based gene deletion and modification in saccharomyces cerevisiae. *Yeast* 14, 953-961 (1998).**
8. **Orr-Weaver, T.L. and Szostak, J.W. Multiple, tandem plasmid integration in saccharomyces cerevisiae. *Mol Cell Biol* 3, 747-749 (1983).**
9. **Calleja, V., Ameer-Beg, S.M., Vojnovic, B., Woscholski, R., Downward, J., and Larijani, B. Monitoring conformational changes of proteins in cells by fluorescence lifetime imaging microscopy. *Biochem J* 372, 33-40 (2003).**
10. **Colman-Lerner, A., Gordon, A., Serra, E., Chin, T., Resnekov, O., Endy, D. et al. Regulated cell-to-cell variation in a cell-fate decision system. *Nature* 437, 699-706 (2005).**
11. **Goldstein, A.L., Pan, X., and McCusker, J.H. Heterologous ura3mx cassettes for gene replacement in saccharomyces cerevisiae. *Yeast* 15, 507-511 (1999).**
12. **Bishop, A.C., Ubersax, J.A., Petsch, D.T., Matheos, D.P., Gray, N.S., Blethrow, J. et al. A chemical switch for inhibitor-sensitive alleles of any protein kinase. *Nature* 407, 395-401 (2000).**
13. **Sikorski, R.S. and Hieter, P. A system of shuttle vectors and yeast host strains designed for efficient manipulation of DNA in saccharomyces cerevisiae. *Genetics* 122, 19-27 (1989).**
14. **Campbell, R.E., Tour, O., Palmer, A.E., Steinbach, P.A., Baird, G.S., Zacharias, D.A. et al. A monomeric red fluorescent protein. *Proc. Natl. Acad. Sci. U. S. A.* 99, 7877-7882 (2002).**
15. **Gordon, A., Colman-Lerner, A., Chin, T., Benjamin, K.R., and Brent, R. Quantification of molecules and reaction rates in single cells with open source microscope based cytometry. *Nature Methods*, *Submitted* (2006).**
16. **Brun, R., Couet, O., Vandroni, C., and Zanarini, O. Paw physics analysis workstation cern program library entry q121. CERN Geneva (1989).**
17. **Meldrum, D.R. and Holl, M.R. Tech.Sight. Microfluidics. Microscale bioanalytical systems. *Science* 297, 1197-1198 (2002).**
18. **Abramoff, M.D., Magelhaes, P.J., and Ram, S.J. Image processing with imagej. *Biophotonics International* 11, 36-42 (2004).**
19. **Newman, J.R., Ghaemmaghami, S., Ihmels, J., Breslow, D.K., Noble, M., Derisi, J.L. et al. Single-cell proteomic analysis of *s. Cerevisiae* reveals the architecture of biological noise. *Nature* DOI:10.1038, 1-7 (2006).**
20. **Black, H.S. Stabilized feed-back amplifiers. *Electrical Engineering* 53, 114-120 (1934).**

[21] **Savageau, M.A. Comparison of classical and autogenous systems of regulation in inducible operons. *Nature* 252, 546-549 (1974).**

[22] **Becskei, A. and Serrano, L. Engineering stability in gene networks by autoregulation. *Nature* 405, 590-593 (2000).**

[23] **Barkai, N. and Leibler, S. Robustness in simple biochemical networks. *Nature* 387, 913-917 (1997).**

[24] **Black, J.W. and Leff, P. Operational models of pharmacological agonism. *Proc. R. Soc. Lond. B Biol. Sci.* 220, 141-162 (1983).**

[25] **Shannon, C. A mathematical theory of communication. *Bell System Technical Journal* 27, 379-423 (1948).**

[26] **Yi, T.M., Kitano, H., and Simon, M.I. A quantitative characterization of the yeast heterotrimeric g protein cycle. *Proc. Natl. Acad. Sci. U. S. A.* 100, 10764-10769 (2003).**

[27] **Oehlen, L.J. and Cross, F.R. G1 cyclins cln1 and cln2 repress the mating factor response pathway at start in the yeast cell cycle. *Genes Dev.* 8, 1058-1070 (1994).**

[28] **Strickfaden, S.C., Winters, M.J., Ben-Ari, G., Lamson, R.E., Tyers, M., and Pryciak, P.M. A mechanism for cell-cycle regulation of map kinase signaling in a yeast differentiation pathway. *Cell* 128, 519-531 (2007).**

[29] **Ma, D., Cook, J.G., and Thorner, J. Phosphorylation and localization of kss1, a map kinase of the saccharomyces cerevisiae pheromone response pathway. *Mol. Biol. Cell* 6, 889-909 (1995).**

[30] **McCaffrey, G., Clay, F.J., Kelsay, K., and Sprague, G.F., Jr. Identification and regulation of a gene required for cell fusion during mating of the yeast saccharomyces cerevisiae. *Mol. Cell Biol..* 7, 2680-2690 (1987).**

[31] **Andersson, J., Simpson, D.M., Qi, M., Wang, Y., and Elion, E.A. Differential input by ste5 scaffold and msg5 phosphatase route a mapk cascade to multiple outcomes. *EMBO J.* 23, 2564-2576 (2004).**

[32] **Hagen, D.C., McCaffrey, G., and Sprague, G.F., Jr. Pheromone response elements are necessary and sufficient for basal and pheromone-induced transcription of the fus1 gene of saccharomyces cerevisiae. *Mol. Cell Biol..* 11, 2952-2961 (1991).**

[33] **Gartner, A., Nasmyth, K., and Ammerer, G. Signal transduction in saccharomyces cerevisiae requires tyrosine and threonine phosphorylation of fus3 and kss1. *Genes Dev.* 6, 1280-1292 (1992).**

[34] **Kranz, J.E., Satterberg, B., and Elion, E.A. The map kinase fus3 associates with and phosphorylates the upstream signaling component ste5. *Genes Dev.* 8, 313-327 (1994).**

[35] **Hasson, M.S., Blinder, D., Thorner, J., and Jenness, D.D. Mutational activation of the ste5 gene product bypasses the requirement for g protein beta and gamma subunits in the yeast pheromone response pathway. *Mol. Cell Biol..* 14, 1054-1065 (1994).**

[36] **Sabbagh, W., Jr., Flatauer, L.J., Bardwell, A.J., and Bardwell, L. Specificity of map kinase signaling in yeast differentiation involves transient versus sustained mapk activation. *Mol.Cell* 8, 683-691 (2001).**

[37] **Bardwell, L., Cook, J.G., Zhu-Shimoni, J.X., Voora, D., and Thorner, J. Differential regulation of transcription: Repression by unactivated mitogen-activated protein kinase kss1 requires the dig1 and dig2 proteins. *Proc. Natl. Acad. Sci. U. S. A.* 95, 15400-15405 (1998).**

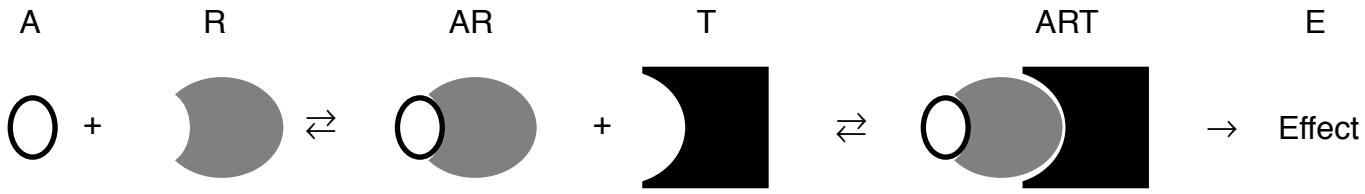
A
R
AR
T
ART
E
+
+
Effect

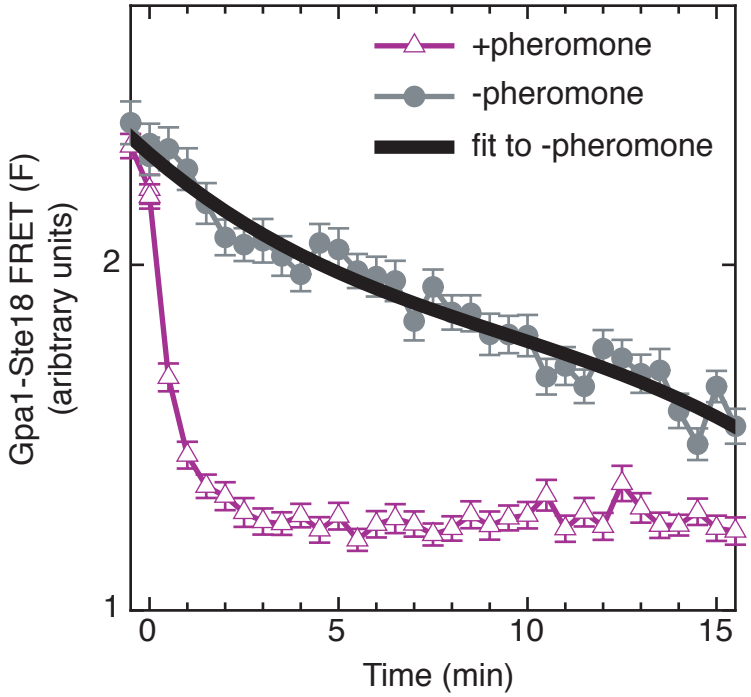
+pheromone
-pheromone
fit to -pheromone
Gpa1-Ste18 FRET (F)
(aribtrary units)
2
1
0
5
10
15
Time (min)

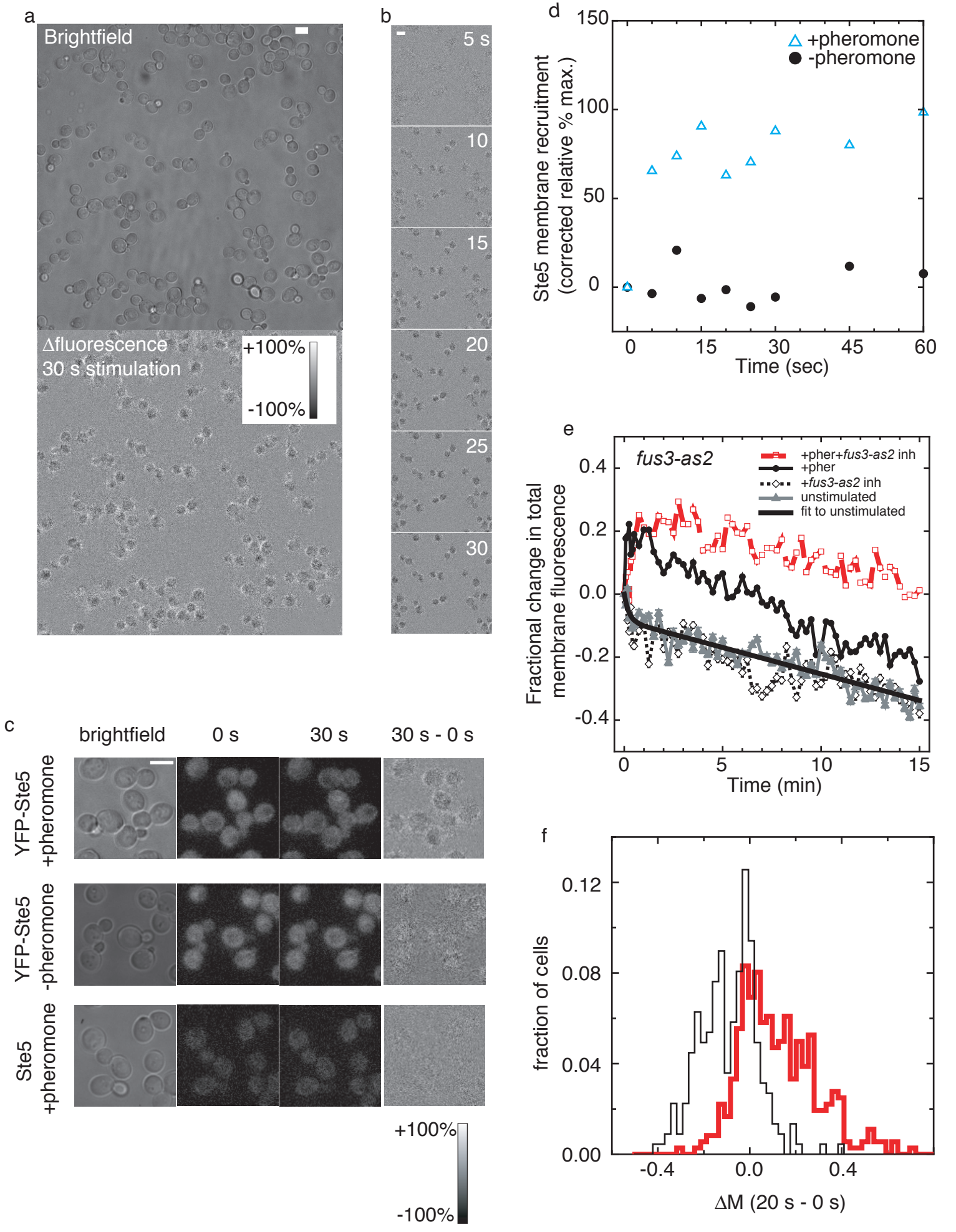
a
Brightfield
Δfluorescence
30 s stimulation
+100%
-100%
b
5 s
10
15
20
25
30
c
brightfield
0 s
30 s
30 s - 0 s
YFP-Ste5
+pheromone
YFP-Ste5
-pheromone
Ste5
+pheromone
+100%
-100%
d
+pheromone
-pheromone
Ste5 membrane recruitment
(corrected relative % max.)
Time (sec)
e
fus3-as2
+pher+fus3-as2 inh
+pher
+fus3-as2 inh
unstimulated
fit to unstimulated
Fractional change in total
membrane fluorescence
Time (min)
f
fraction of cells
ΔM (20 s - 0 s)

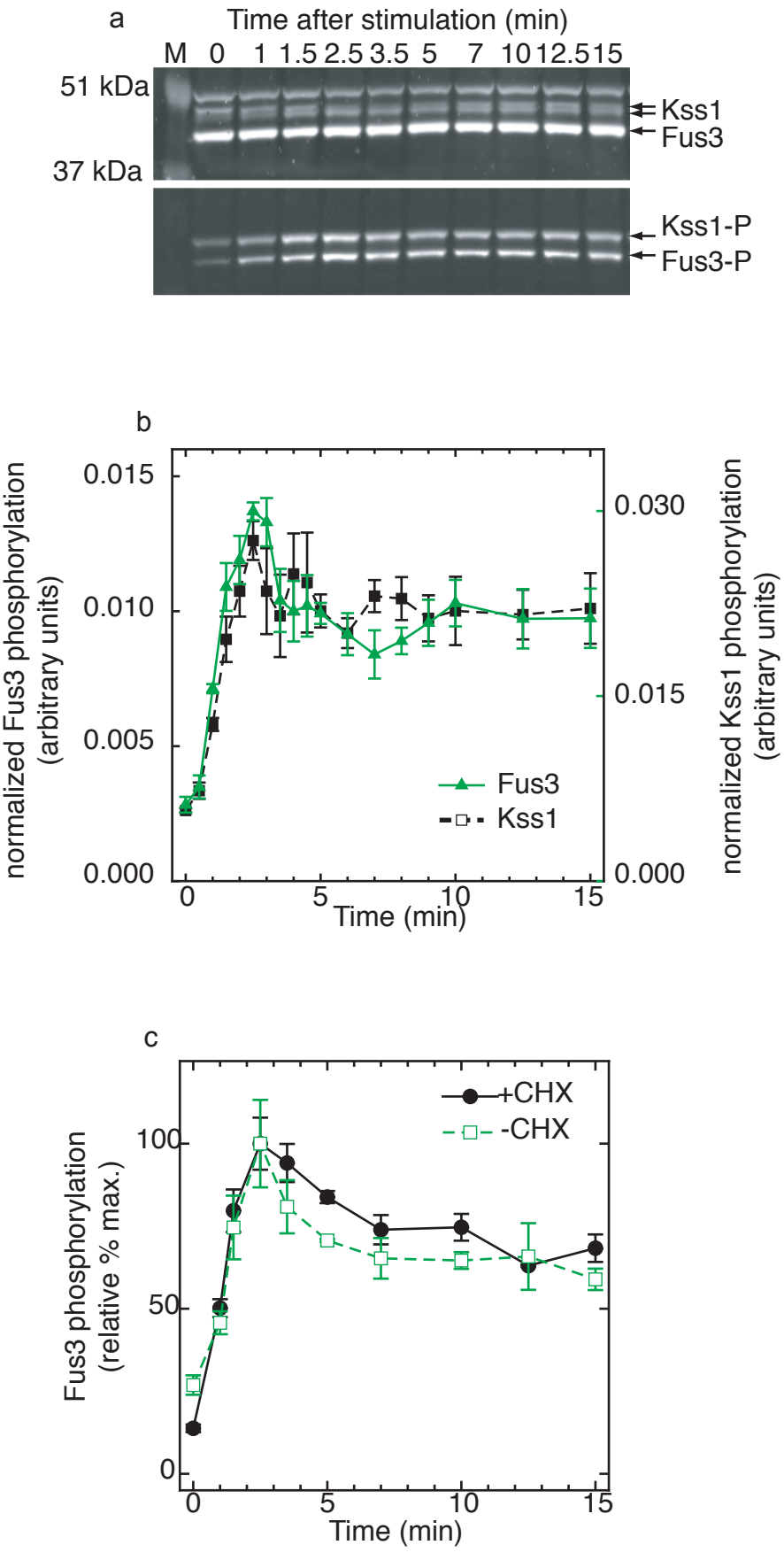
a
Time after stimulation (min)
M 0 1 1.5 2.5 3.5 5 7 10 12.5 15
51 kDa
37 kDa
Kss1
Fus3
Kss1-P
Fus3-P
b
normalized Fus3 phosphorylation (arbitrary units)
normalized Kss1 phosphorylation (arbitrary units)
0.015
0.010
0.005
0.000
0.030
0.015
0.000
0
5
10
15
Time (min)
Fus3
Kss1
c
Fus3 phosphorylation (relative % max.)
100
50
0
+CHX
-CHX
0
5
10
15
Time (min)

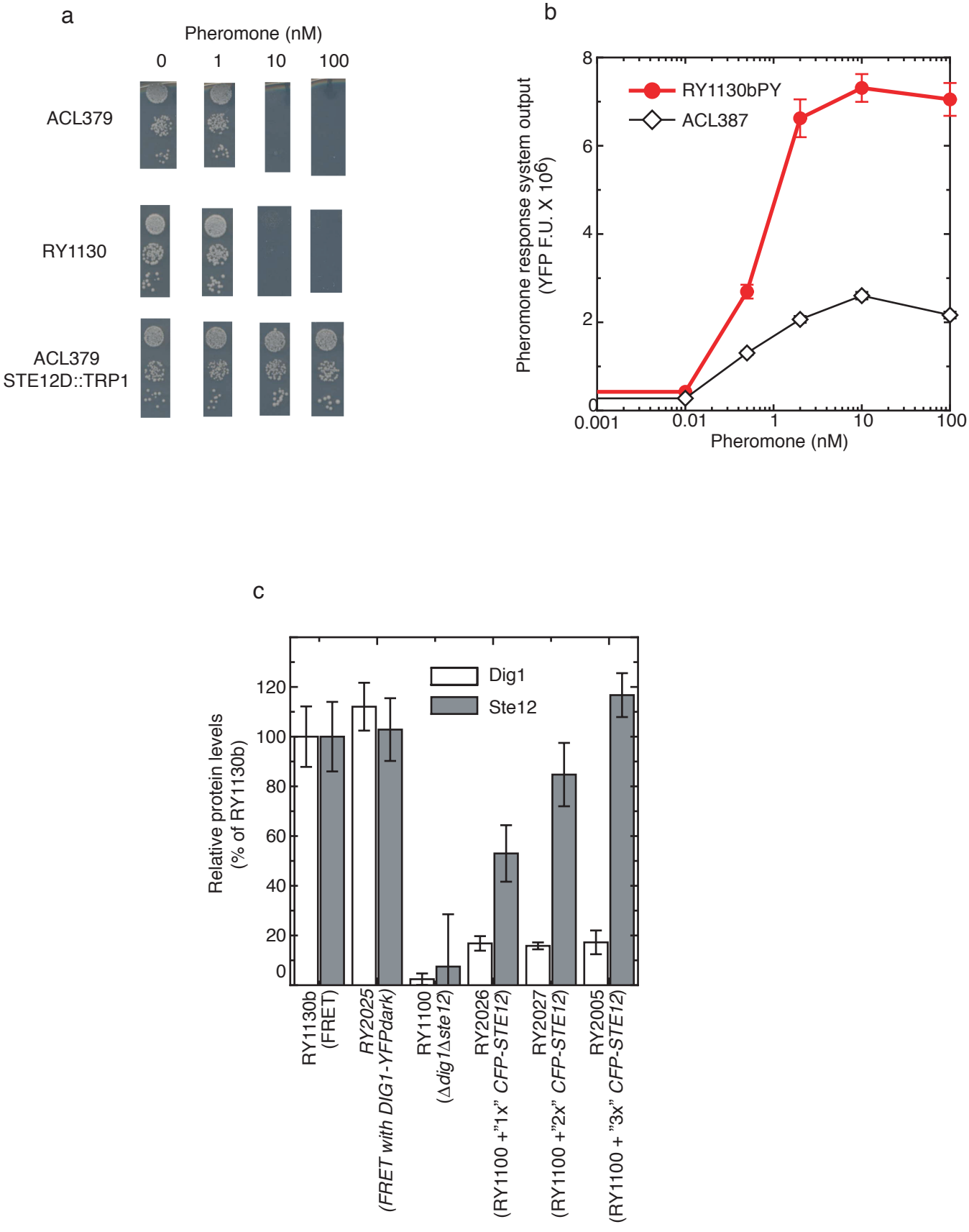
a
Pheromone (nM)
0
1
10
100
ACL379
RY1130
ACL379
STE12D::TRP1
b
Pheromone response system output
(YFP F.U. X 10^6)
RY1130bPY
ACL387
Pheromone (nM)
0.001
0.01
1
10
100
c
Relative protein levels
(% of RY1130b)
Dig1
Ste12
RY1130b
(FRET)
RY2025
(FRET with DIG1-YFPdark)
RY1100
(Δdig1Δste12)
RY2026
(RY1100 +"1x" CFP-STE12)
RY2027
(RY1100 +"2x" CFP-STE12)
RY2005
(RY1100 + "3x" CFP-STE12)

a

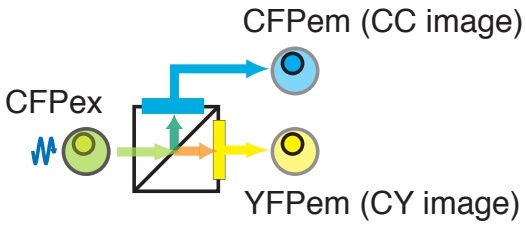

b

Identify cell boundaries

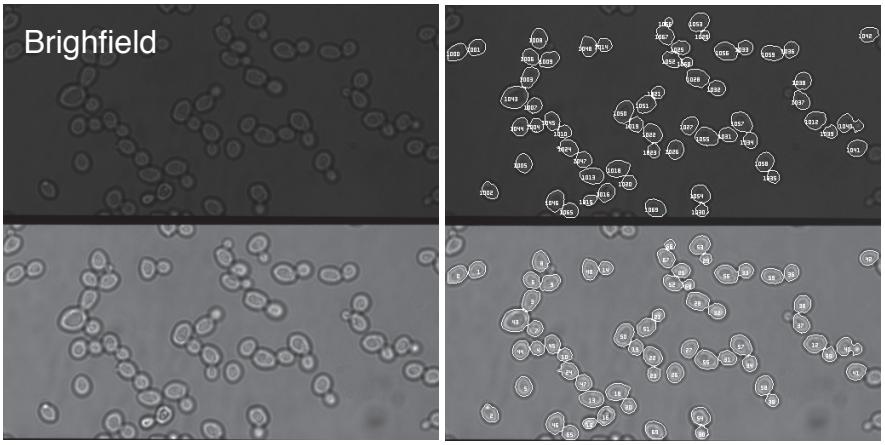

Identify nuclear position and measure acceptor fluorescence (YY)

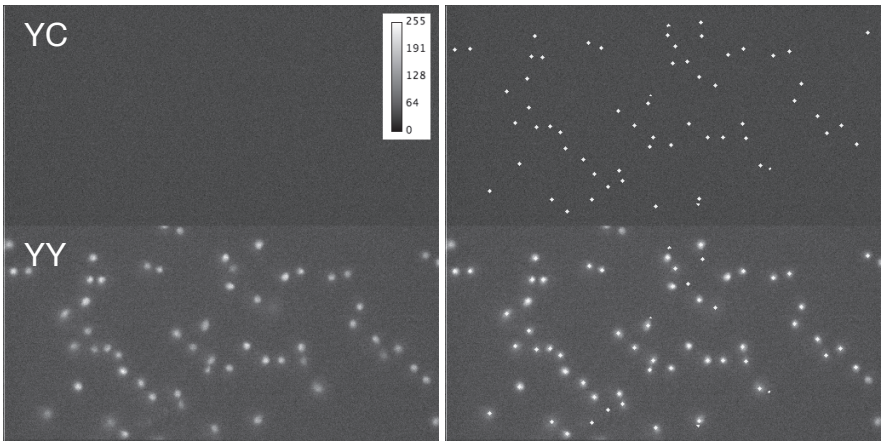

Measure nuclear donor fluorescence (CC) and FRET (CY)

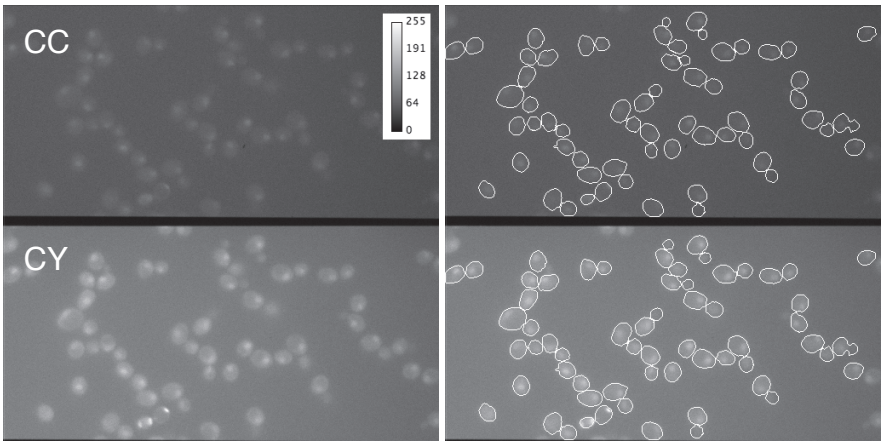

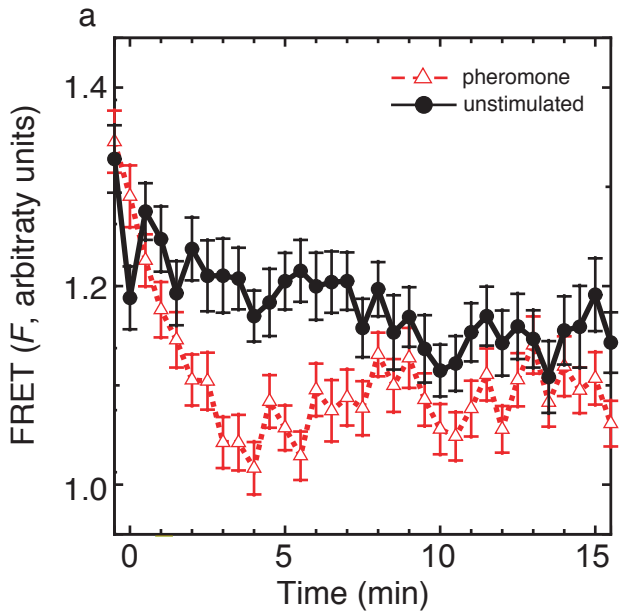
a
pheromone
unstimulated
FRET (F, arbitraty units)
Time (min)

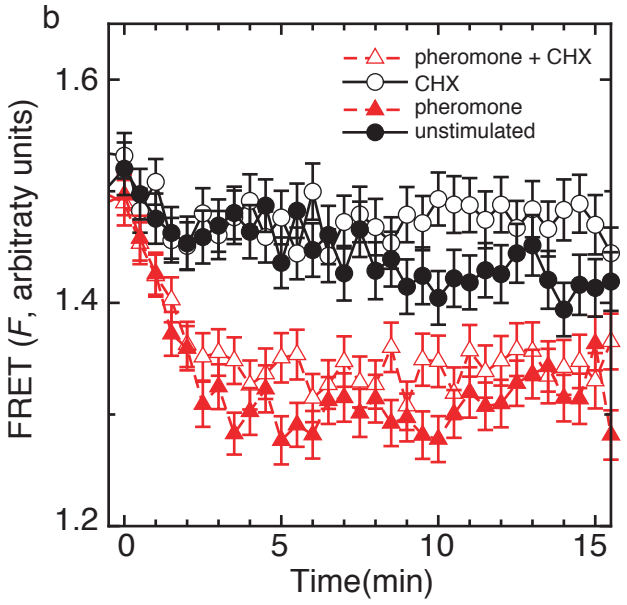
b
pheromone + CHX
CHX
pheromone
unstimulated
FRET (F, arbitraty units)
Time(min)

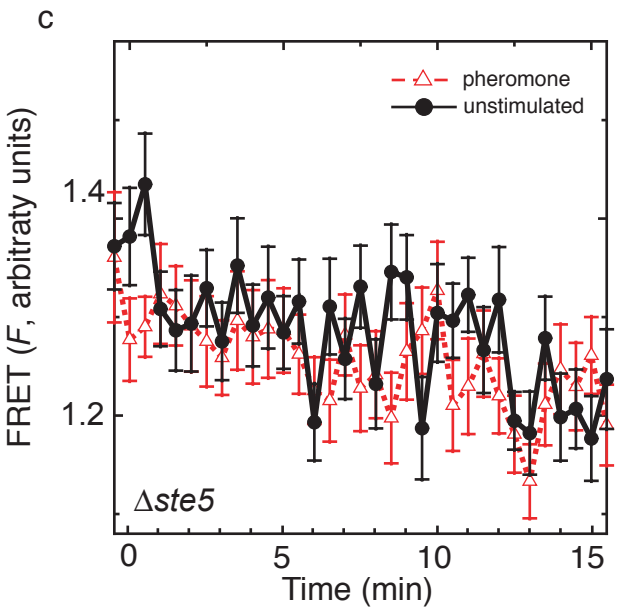
c
pheromone
unstimulated
Δste5
FRET (F, arbitraty units)
Time (min)

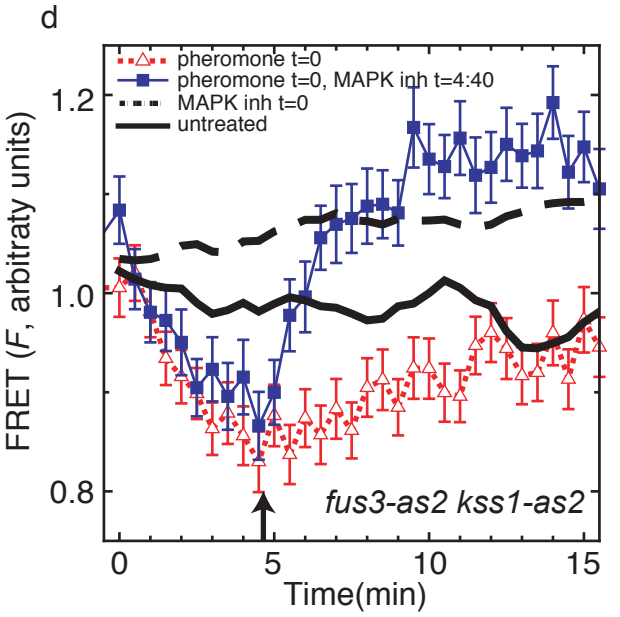
d
pheromone t=0
pheromone t=0, MAPK inh t=4:40
MAPK inh t=0
untreated
fus3-as2 kss1-as2
FRET (F, arbitraty units)
Time(min)

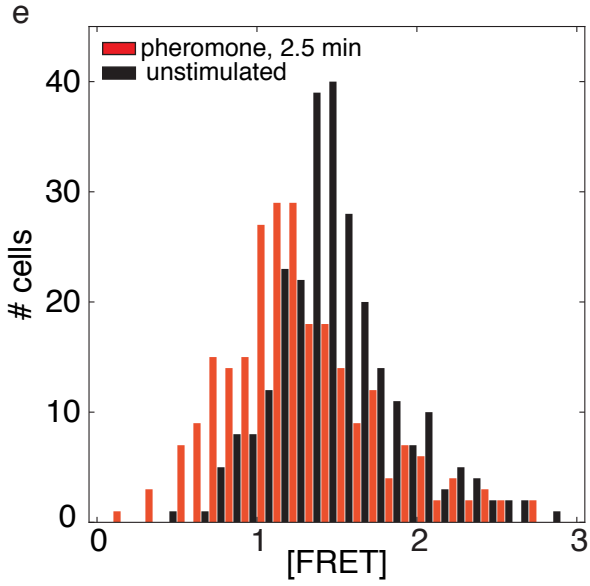
e
pheromone, 2.5 min
unstimulated
cells
[FRET]

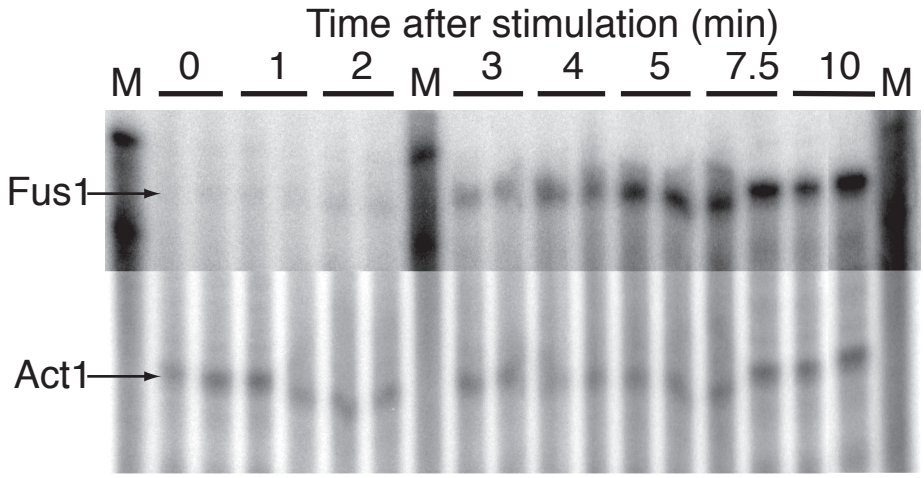
Time after stimulation (min)
M
0
1
2
M
3
4
5
7.5
10
M
Fus1
Act1

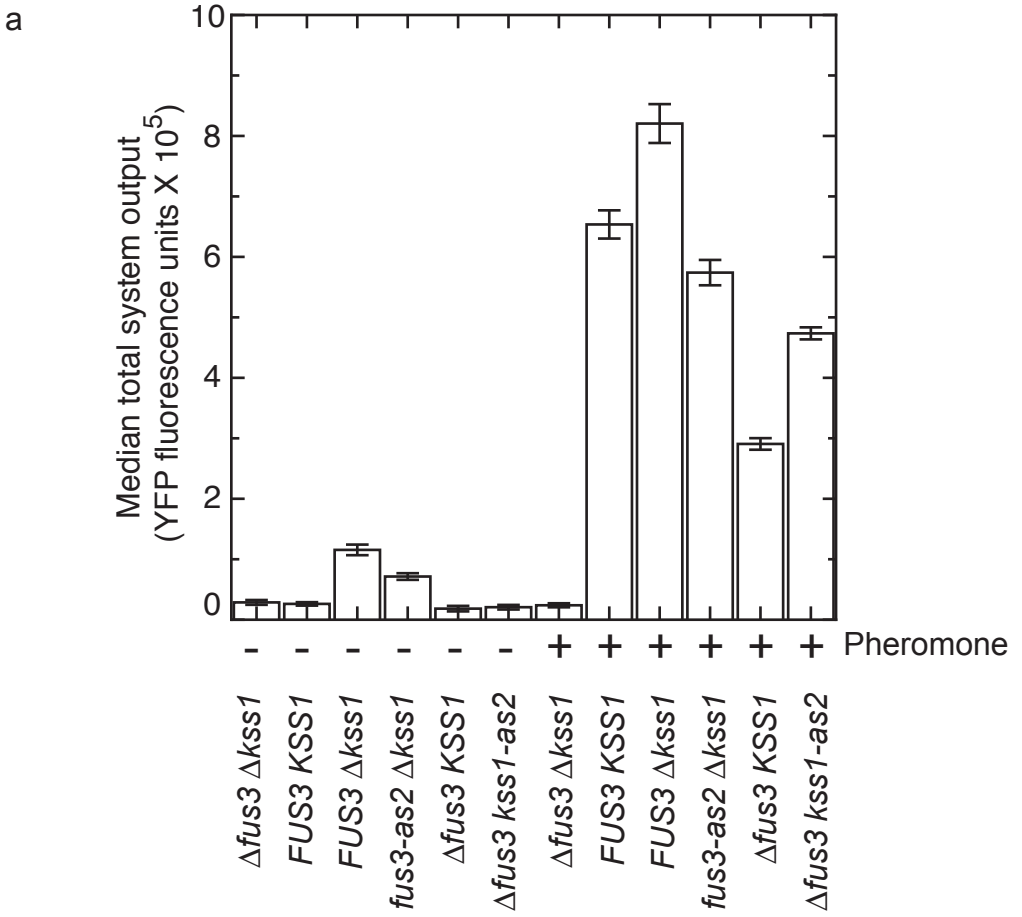
a
Median total system output
(YFP fluorescence units X 10^5)
10
8
6
4
2
0
- - - - - - + + + + + +
Pheromone
Δfus3 Δkss1
FUS3 KSS1
FUS3 Δkss1
fus3-as2 Δkss1
Δfus3 KSS1
Δfus3 kss1-as2
Δfus3 Δkss1
FUS3 KSS1
FUS3 Δkss1
fus3-as2 Δkss1
Δfus3 KSS1
Δfus3 kss1-as2

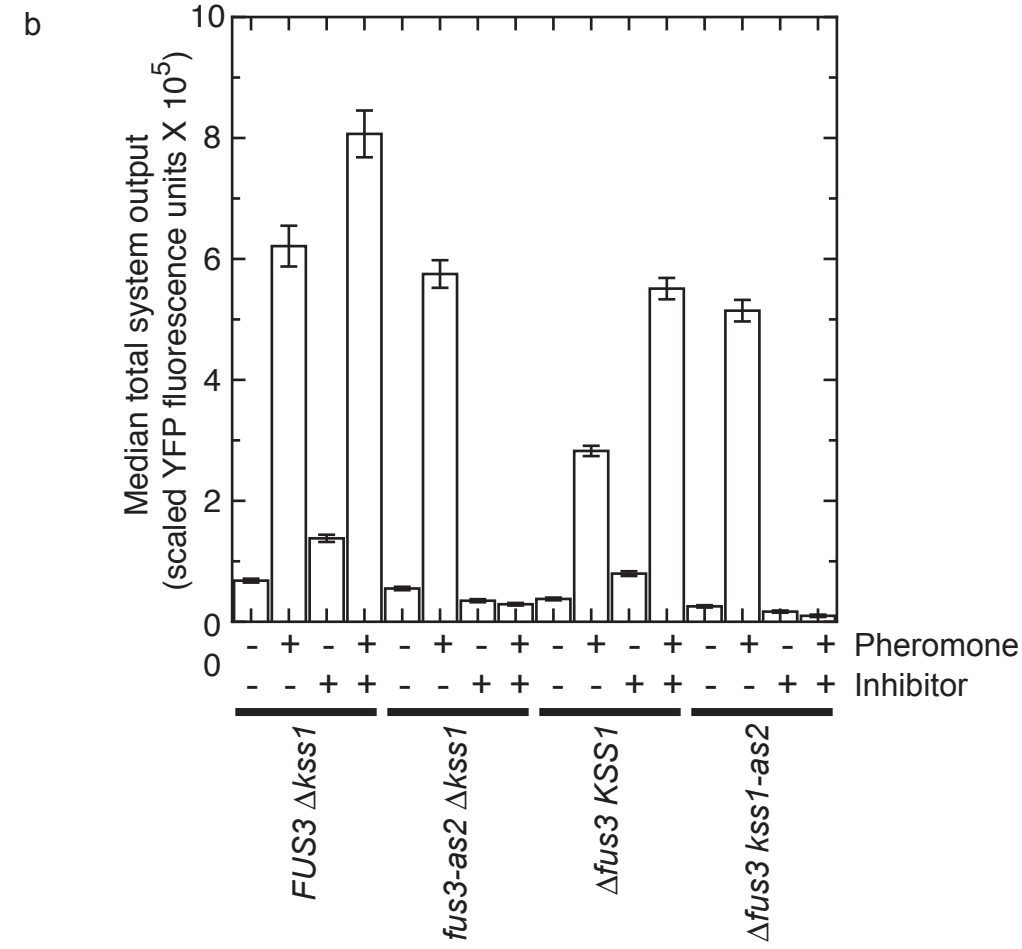
b
Median total system output
(scaled YFP fluorescence units X 10^5)
10
8
6
4
2
0
0
- + - + - + - + - + - + - + - +
Pheromone
- - + + - - + + - - + + - - + +
Inhibitor
FUS3 Δkss1
fus3-as2 Δkss1
Δfus3 KSS1
Δfus3 kss1-as2

RY2062b
(TMY101 *fus3-as2*)

TMY101

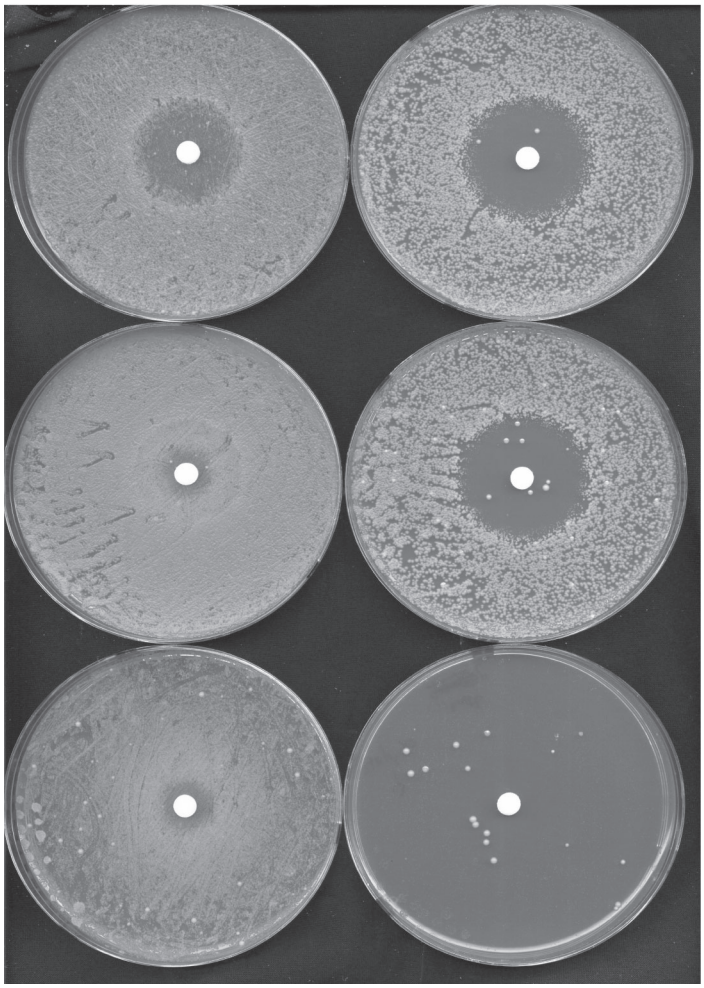

Plate: YAPD
Disc: Pheromone

Plate: YAPD
Disc: Pheromone + inhibitor

Plate: YAPD + 100 nM pheromone
Disc: inhibitor

a

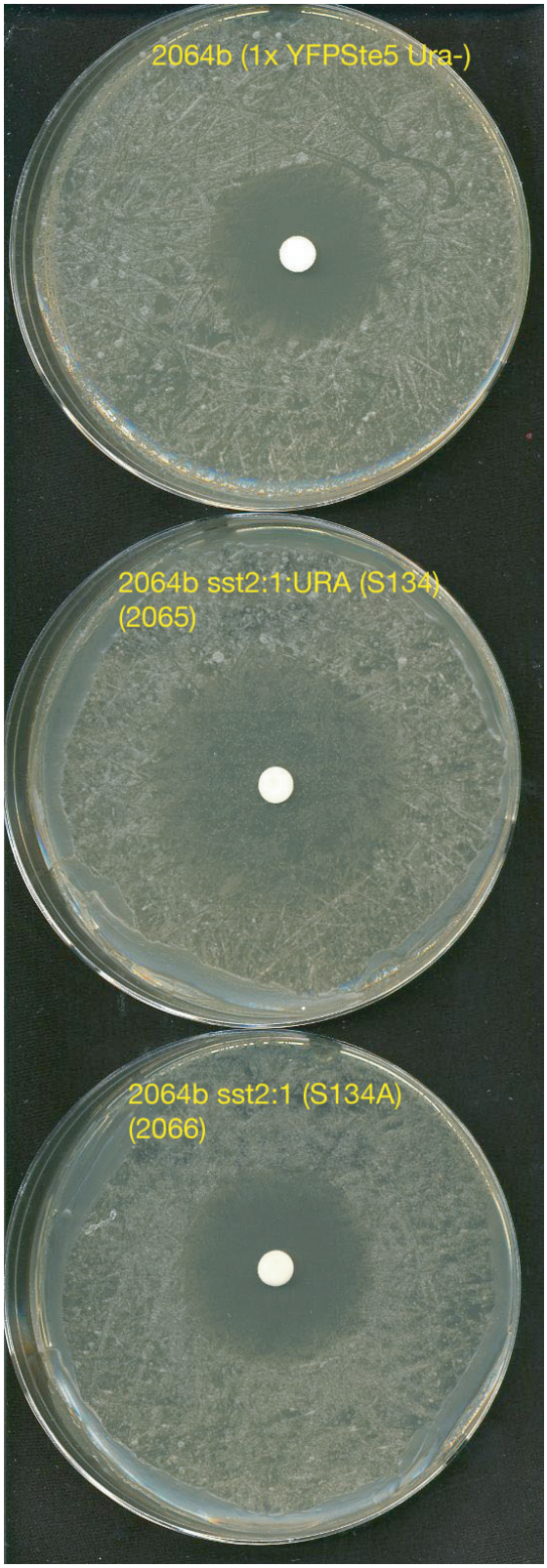
2064b (1x YFPSte5 Ura-)
2064b sst2:1:URA (S134)
(2065)
2064b sst2:1 (S134A)
(2066)

b

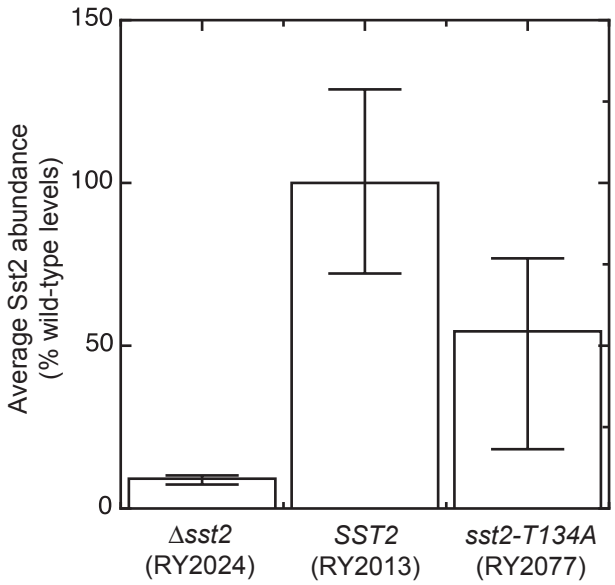
150
100
50
0
Average Sst2 abundance
(% wild-type levels)
Δsst2
(RY2024)
SST2
(RY2013)
sst2-T134A
(RY2077)

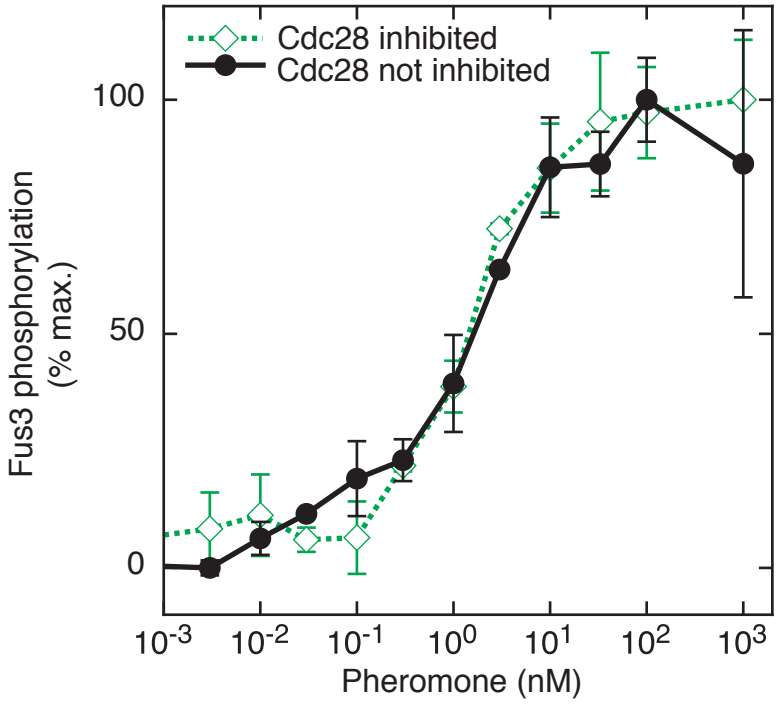
Cdc28 inhibited
Cdc28 not inhibited
Fus3 phosphorylation
(% max.)
100
50
0
10-3
10-2
10-1
100
101
102
103
Pheromone (nM)

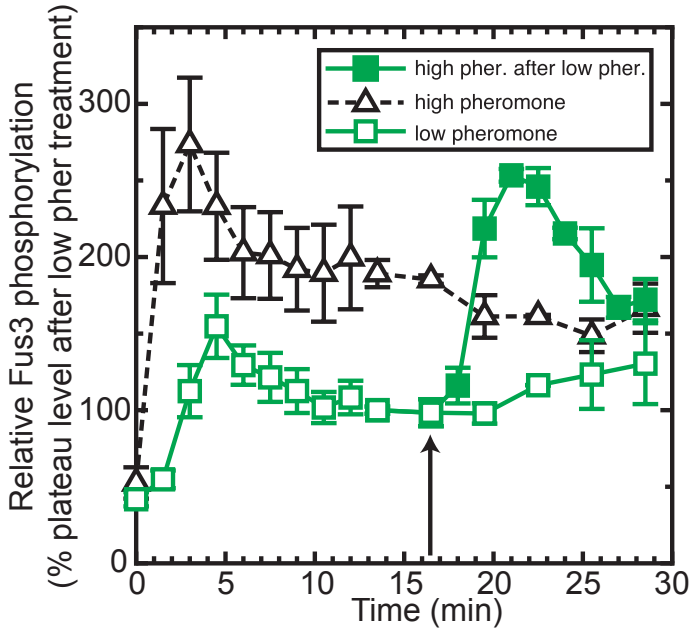
high pher. after low pher.
high pheromone
low pheromone
Relative Fus3 phosphorylation
(% plateau level after low pher treatment)
0
100
200
300
0
5
10
15
20
25
30
Time (min)

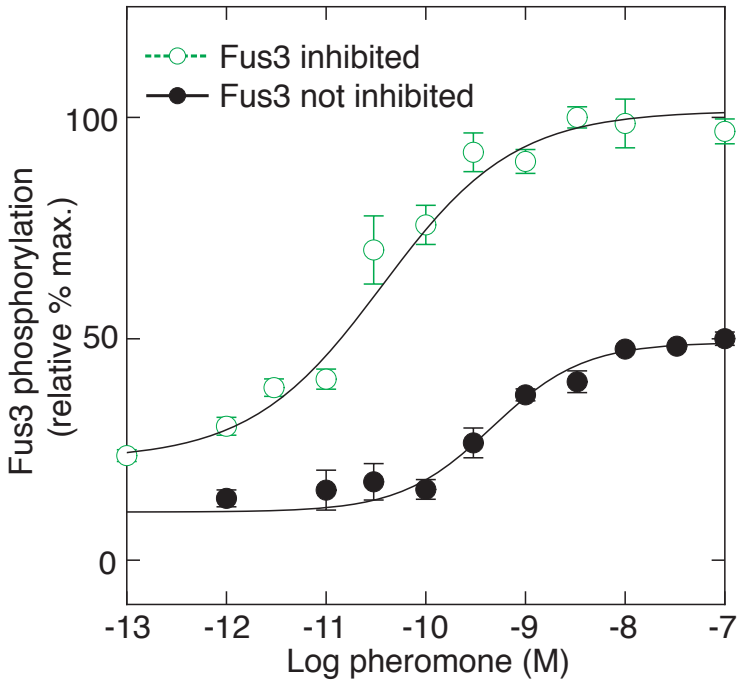
Fus3 inhibited
Fus3 not inhibited
Fus3 phosphorylation
(relative % max.)
100
50
0
-13
-12
-11
-10
-9
-8
-7
Log pheromone (M)